T-4076

RADIAL GROWTH, MODAL AND KINETIC ANALYSIS OF HIGH SPEED ROTORS

by

Michael S. DeBruzzi

T-4076

A thesis submitted to the Faculty and the Board of Trustees of the Colorado School of Mines in partial fulfillment of the requirements for the degree of Master of Science (Applied Mechanics).

Golden, Colorado

Date 6 Nov, 1991

Signed: Michael S DeBruzzi
Michael S. DeBruzzi

Approved: Robert C Hansen
Dr. Robert C. Hansen
Thesis Advisor

Golden, Colorado

Date 8 Nov. 1991

Joan Gosink
Dr. Joan Gosink
Department Head,
Engineering Department

ABSTRACT

There exist several problems which must be overcome in the successful design of high speed rotors which are rigid with respect to bending and compliantly supported. Radial growth compatibility between the rotor and its supports must be precisely calculated, in order to determine the required static dimensions of the critical components. In the modal analysis natural frequencies are identified by solving for the homogeneous solution of the differential equations of motion which describe the system. Kinetic analysis employs the radial growth and modal analyses, in order to accurately calculate the particular solution or forced response of the two-degree-of-freedom, spring-mass (2 DOF) system. The force used in the kinetic analysis is a result of the eccentric force generated by rotor imbalance. Numerical and analytical methods are employed in several aspects of the analysis with very good correlation, demonstrating that similar results can be attained using different mathematical techniques. Experimental data in support of the techniques presented in this document will be acquired in future prototype testing.

TABLE OF CONTENTS

	Page
ABSTRACT	iii
LIST OF FIGURES	vi
LIST OF SYMBOLS	viii
ACKNOWLEDGMENTS	xii
Chapter	
1. INTRODUCTION	1
2. RADIAL GROWTH ANALYSIS	6
2.1 Radial Deformation Due to Centrifugal Force	7
2.2 Radial Deformation Due to Assembly Interference Fit	9
2.3 Remarks	12
3. MODAL ANALYSIS	14
3.1 Natural Frequency Calculations	16
3.1.1 Numerical Techniques	17
3.1.2 Analytical Techniques	18
3.2 Gyroscopic Stiffening	28
3.3 Eigenvector Calculations	33
3.4 Forced Vibration Magnification Factor	36
3.5 Forced Vibration Phase Angle	37
3.6 Remarks	38
4. KINETIC ANALYSIS	39
4.1 Lever Rule	41
4.2 Centrifugal Force	42
4.3 Moments Generated by Centrifugal Force	47
4.4 Gyroscopic Stabilization	49
4.5 Remarks	53
5. APPLICATION OF THEORIES	57

5.1 Rotor Configurations 58
5.2 Radial Deformation 61
5.3 Small Angle Approximation 68
5.4 Natural Frequencies 69

5.4.1 First Rotor 70
5.4.2 Second Rotor 75

5.5 Dynamic System Factors 78
5.6 Kinetic Effects 80

5.6.1 First Rotor 81
5.6.2 Second Rotor 85

5.7 Radial Clearance Including Kinetic Effects 87
5.8 Remarks 94

6. CONCLUSIONS 95

6.1 Analytical Remarks 95
6.2 Future Work 98

. . . . . .

REFERENCES CITED 100

LIST OF FIGURES

Figure		Page
2.1	Rotor/Bearing Interface	6
3.1	Modal Description	16
3.2	Rotor Model	20
3.3	Axis System of Gyroscopic Element	29
4.1	Graphic Representation of The Lever Rule	42
4.2	Eccentricity of Rigidly Supported, Rigid Rotor	43
4.3	Eccentricity of Compliantly Supported, Rigid Rotor	44
4.4	Free-Body Diagram of Rotor	50
4.5a	Possible Boundary Conditions Applicable to the Compliantly Mounted, Rigid Rotor With Limited Deflection	55
4.5b	Possible Boundary Conditions Applicable to the Compliantly Mounted, Rigid Rotor With Limited Deflection (cont.)	56
5.1	Simplified First Rotor Cross-Section	58
5.2	Simplified Second Rotor Cross-Section	60
5.3	Discrete Rotor Sections	62
5.4	FEA of 3-D Rotor Section With Magnets, Rotating at 30,000 RPM	64
5.5	FEA of Axisymmetric Rotor With Magnets, Rotating at 30,000 RPM	66
5.6	FEA of Axisymmetric Rotor With No Magnets, Rotating at 30,000 RPM	67
5.7	Maximum Rotor Angular Deflection	69
5.8	First Rotor Magnification Factors	72

5.9 Speed Dependence of the First Rotor Natural Frequencies 73

5.10 Second Rotor Magnification Factors 75

5.11 Speed Dependence of the Second Rotor Natural Frequencies 77

5.12 First Rotor Phase Angles 79

5.13 Second Rotor Phase Angles 80

5.14 First Rotor Reaction Forces 81

5.15 First Rotor Reaction Forces, If Excessive Static Radial Clearance Exists 85

5.16 Second Rotor Reaction Forces 86

5.17 Available and Floating Clearance 88

5.18 First Rotor Radial Clearance at Position A 89

5.19 First Rotor Radial Clearance at Position B 90

5.20 Second Rotor Radial Clearance at Position A 91

5.21 Second Rotor Radial Clearance at Position B 91

LIST OF SYMBOLS

A	Location of one rotor support (bearing)
a	Axial distance separating the rotor mass center from "A" (in.)
B	Location of the other rotor support (bearing)
b	Axial distance separating the rotor mass center from "B" (in.)
C	Location of the rotor centroid
E	Elastic modulus (psi.)
e	Static rotor eccentricity (in.)
e_{tot}	Total rotor eccentricity (including deflection of compliant rotor supports, (in.))
e_y	"Y" component of compliant rotor support deflection (in.)
e_z	"Z" component of compliant rotor support deflection (in.)
F	Force (lbs)
F_{eff}	Effective force (including magnification factor)
G	Location of the rotor mass center
g	Gravitational constant (386.6 in/sec^2)
in.	inches
I	Mass moment of inertia (in-lb-sec^2)
I_x	Mass moment of inertia about an axis perpendicular to the spin axis (in-lb-sec^2)
I_z	Mass moment of inertia about the spin axis (in-lb-sec^2)

K_1	Stiffness of one rotor support (in/lb)
K_2	Stiffness of the other rotor support (in/lb)
[K]	Stiffness matrix (2 x 2)
K_g	Gyroscopic stiffness (in-lb/radian).
KHz	Frequency (thousand Hertz)
KSI	Stress (thousand pounds per square inch)
lbs	Weight (pounds)
[M]	Mass matrix (2 x 2)
m	Mass (lb-sec^2/in.)
MF_t	Magnification factor associated with the translation natural frequency
MF_w	Magnification factor associated with the wobble natural frequency
O	Geometric bearing center.
p_i	Pressure acting on the inner surface of a cylinder (PSI)
p_o	Pressure acting on the outer surface of a cylinder (PSI)
PSI	lbs/in^2
RPM	Revolutions per minute
r_i	Inner radius (in.)
r_o	Outer radius (in.)
r_r	Reference radius (in.)
T_z	Moment (or torque) about the "z" axis
u	Radial deformation (in.)

Wt	Weight (lbs)
x	Distance in "x" direction (in.)
y	Distance in "y" direction (in.)
Δy_a	Transverse deflection of the rotor principal centroidal axis, at location "A" (in.)
Δy_b	Transverse deflection of the rotor principal centroidal axis, at location "B" (in.)
Δy_c	Transverse deflection of the rotor principal centroidal axis, at the rotor mass center (in.)
$\ddot{y}$	Linear acceleration in the "y" direction (in/sec^2)
z	Distance in the "z" direction (in.)

GREEK

ϕ	Phase angle (degrees)
λ	Natural frequency squared (ω_n^2)
θ_x	Angular displacement about the "x" axis
θ_y	Angular displacement about the "y" axis
θ_z	Angular displacement about the "z" axis
ν	Poison's Ratio
ρ	Weight density (lb/in^3)
σ_r	Stress in the radial direction (PSI)
σ_θ	Stress in the circumferential direction (PSI)
ω	Angular velocity (RPM or radians per second)
ω_d	Damped natural frequency (RPM)
ω_n	Natural frequency (RPM)
ω_x	Angular velocity about the "x" or spin axis (RPM or radians per second)

ACKNOWLEDGMENTS

It is appropriate to acknowledge those responsible for the success of this endeavor in a chronological fashion. The Department of Veterans Affairs has provided the primary financial support necessary for completion of course work and thesis. Without this support, my dedication to this project would not have been possible.

Professor John P.H. Steele made possible my association with Unique Mobility Inc. Unique Mobility provided the invaluable opportunity of direct and extended contact with Dr. Paul Y. Kim, Research Officer, National Research Council of Canada (NRCC).

Alcan International Ltd. and Unique Mobility have jointly provided a significant amount of financial support necessary for the development of the analytical techniques presented in this document. The rotor configurations presented are the result of significant engineering input by Dr. Ralph Flanagan (University of Ottawa), Dr. Paul Y. Kim (NRCC), Dr. Hao Huang, Mr. Joseph Olbermann, Mr. Jon Scull and myself (Unique Mobility).

Each and every one of my professors at the Colorado School of Mines has provided valuable perspectives that were employed in this analysis. My thesis committee members, Dr.

Robert C. Hansen, Dr. John P.H. Steele and Dr. David Matlock have graciously given of their time whenever necessary. My wife, Shanna, and my children have endured my excessive absence (and occasionally tolerated my presence) while in pursuit of this goal. Lacking any of the people, institutions or events mentioned above, the following analysis would not have been possible. I thank you all.

Chapter 1

INTRODUCTION

It has been proposed that an electric powered flywheel could be designed to act as a mechanical energy storage device in an electric vehicle. This device would be capable of converting between mechanical and electrical energy at a higher rate than any presently available battery storage system can convert between chemical and electrical energy. Because of this high rate of energy conversion, the energy that is presently being dissipated as heat in the vehicle's braking system could be stored in the flywheel as rotational kinetic energy. This energy would then be used to accelerate the vehicle at a later time. Under certain driving conditions, this scheme could extend the range of a conventional electric vehicle. Although it is not clear that range will always be extended, it has been predicted that the vehicle will be capable of higher performance levels without decreasing battery life (1).

In order for the system to be practical, it was determined that the rotor must be capable of angular velocities as high as 30,000 RPM. In addition, the rotor will have significant inertia about its axis of rotation. Therefore, the system will be capable of storing a large amount of energy (approximately 500 W-h). Rotating parts are common in mechan-

ical systems. The rotor in a turbo-charger for an internal combustion engine is capable of angular velocities much greater than 30,000 RPM, but these devices have relatively little inertia. The flywheels of some internal combustion engines have significant inertia, but rotate at relatively low speeds.

In rotors that have high inertia and rotate at high speed, there are common phenomena that will have significant effects on system operation. Among these phenomena are radial growth compatibility of rotating members, system natural frequencies (or critical speeds), and gyroscopic effects. The definition of "high speed" is not clear because this description is relative to each particular system. High speed in one system could be 1,000 RPM, while in another system it could be 100,000 RPM. High speed could be defined as operational speeds greater than the first critical speed of the particular rotor system.

Eshleman (2) has provided a precise and descriptive definition of critical speed. "If the frequency of any harmonic component of a periodic forcing phenomenon is equal to, or approximates, the frequency of any mode of rotor vibration, a condition of resonance may exist; if resonance exists at a specific speed, that speed is called a critical speed." Resonant conditions can exist at natural frequencies. It is assumed that the rotor is isolated from externally

originated vibrations. Therefore, if there exists a forcing function whose frequency varies with rotor angular velocity (such as rotor imbalance), and it does not induce resonance at a rotor natural frequency, then that natural frequency is not a critical speed.

All rotor systems will exhibit these phenomena to certain degrees. In some systems, radial growth compatibility problems can be overcome by assembling the parts with a static interference fit, or by providing an elastic interface between critical components. In other systems, dynamic problems can be overcome by adjusting the stiffness of critical components, providing appropriate damping, or by a combination of these techniques. Gyroscopic effects tend to stabilize rotor systems by making them resistant to angular displacement of the principal centroidal axis. This change in resistance will affect the system natural frequencies. A thorough knowledge of each of these phenomena is essential to accurately predicting rotor dynamic characteristics.

Preliminary dynamic system calculations of the initially proposed rotor revealed that a natural frequency would exist at approximately 30,100 RPM. It is likely that this natural frequency would have been a critical speed. In addition, it was found that it is not possible to maintain contact between the rotor inner surface and the bearing outer races, without providing an elastic interface between them. It was deter-

mined that catastrophic failure would have been imminent for the initially proposed configuration, within its operating speed range.

Modifications were proposed to account for the dynamic system and radial growth compatibility problems. It appears as if the proposed modifications will produce a marginally stable system (as opposed to an unstable system). In this case, marginal stability implies that under certain operating conditions, which could be considered to be normal, rotor instability could be induced, followed by premature system failure. It has become obvious that the system will be highly sensitive to dimensional tolerances of critical components. In order to determine the limits of the dimensional tolerances, an algorithm was developed to compute the steady-state bearing reaction forces generated by the rotor eccentricity, as a function of rotor angular velocity. A Fortran computer program was then written for machine computation of solutions.

The following analysis is divided into four sections. Chapter Two presents the analytical and numerical methods of computing stress and radial deformation in axisymmetric, rotating members. In the numerical method, the commercially available Algor Finite Element Analysis software (Algor or FEA) was used. Chapter Three consists of the modal analysis of a two degree of freedom spring-mass rotor system. Prior to

applying the techniques developed in the modal analysis section, it is necessary to determine that the rotor being analyzed can be considered to be rigid (it does not need to be rigidly supported.) Chapter Four consists of the kinetic analysis of a rotor with the proposed configuration. And Chapter Five contains an application of the theories to two different rotor systems. These systems possess significantly different dynamic properties, and appropriately, they exhibit significantly different dynamic response.

It is noteworthy that the following analysis has not been experimentally proven. However, in several instances analytical and numerical techniques were employed to find the solution. Very good correlation was realized between the different mathematical techniques. In addition, the results produced appear to be accurate and logical, using the analytical techniques presented. Several cross-checks are presented in Chapter Five as evidence of proper analytical solution techniques. These checks provide a degree of confidence in the algorithm, by demonstrating that there are no obvious violations of the laws of mechanics.

Chapter 2

RADIAL GROWTH ANALYSIS

There are two reasons why radial growth analysis of the rotor critical components is essential to a complete system analysis. First, if the bearing outer race is rotating with the rotor and the inner race is stationary, then at some speed the rotor inner radius will be greater than the outer radius of the bearing race (see Figure 2.1). Relative motion between the rotor and bearing outer race could result in catastrophic failure due to excessive bearing loads, if that speed is within the proposed operating range. Second, if radial

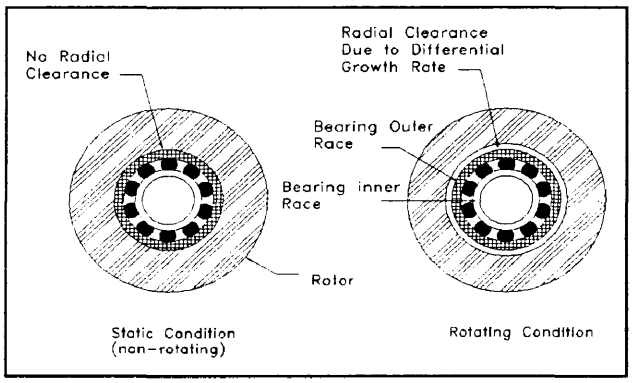

Figure 2.1: Rotor/Bearing Interface

clearance exists between the bearing outer race and the rotor inner surface, and the two surfaces are separated by an elastic interface, then in order to determine the steady-state rotor support reaction forces, it is necessary to know how

much radial clearance exists between the rotor inner surface and bearing outer race, as a function of rotor angular velocity.

2.1 Radial Deformation Due to Centrifugal Force

Linear elastic, radial deformation and the state of stress in many rotors, which are due to centrifugal loading conditions, can be computed using generalized analytical solutions that are based on the "axisymmetric disk" rotor geometry. The term "analytical solution" refers to the closed-form integration of the differential equation which describes the respective phenomenon, including the application of the appropriate boundary conditions. For more complex rotor geometries, where the derivation of an analytical solution is not convenient, a combination of numerical and generalized analytical solution techniques constitutes a complete radial growth analysis. Equation 2.1 defines the radial deformation in an axisymmetric disk, as a function of radius (3). It is important to note that if the rotor is not disk shaped, it is not necessarily valid to use Equations 2.1 through 2.3 to describe the radial deformation and the state of stress in the rotor.

$$u = \frac{\rho r_r \omega^2 (3+\nu)}{8Eg}\left[(r_i^2+r_o^2)(1-\nu) + \frac{r_i^2 r_o^2}{r_r^2}(1+\nu) - \left(\frac{1-\nu^2}{3+\nu}\right) r_r^2\right]$$

Equation 2.1: Radial Deformation Due to Centrifugal Loading Conditions

It is necessary to know precisely the uniaxial equivalent stress in the rotor. If the stress is greater than the material yield stress, rotor failure could occur (depending on the location and degree of yielding). It is likely that the rotor will become significantly more unbalanced or a structurally critical fatigue loading condition could result. Fatigue failure at stress levels as high as the yield stress would probably be characterized as low cycle fatigue. Predictions of fatigue life are more appropriately based on a combination of the material fatigue limit, and either ultimate or yield strength (4). It is beyond the scope of this analysis to actually compute the fatigue behavior of this system. To enhance the degree of confidence in the FEA modelling, uniaxial equivalent stress that is computed in the FEA can be compared with the stress computed using the solutions for the axisymmetric disk.

The uniaxial equivalent stress in an axisymmetric rotating disk can be adequately computed using the stress components acting in the radial and circumferential directions. Equations 2.2 and 2.3 define the radial and

circumferential stress in an axisymmetric disk, as functions of radius (3).

$$\sigma_r = \rho\omega^2\left(\frac{3+\nu}{8g}\right)\left(r_i^2 + r_o^2 - \frac{r_i^2 r_o^2}{r_r^2} - r_r^2\right)$$

Equation 2.2: Radial Stress Due to Centrifugal Loading Conditions

$$\sigma_\theta = \rho\omega^2\left(\frac{3+\nu}{8g}\right)\left[r_i^2 + r_o^2 + \frac{r_i^2 r_o^2}{r_r^2} - \left(\frac{1+3\nu}{3+\nu}\right) r_r^2\right]$$

Equation 2.3: Circumferential Stress Due to Centrifugal Loading Conditions

The stress values generated using these equations can be used with the applicable combined stress criteria (typically either the maximum shear stress or octahedral shear stress criteria), to develop the uniaxial equivalent stress at a particular point of interest in the rotor (r_r).

2.2 Radial Deformation Due to Assembly Interference Fit

Any time an interference fit exists between two assembled axisymmetric parts, a pressure will exist between the two contact surfaces. An internal pressure will be exerted on the external part, and an external pressure will be exerted on the internal part. This will cause a change in the radial dimensions of each. The radius of the external part will become larger and the radius of the internal part will become smaller

than it was in the unassembled state. The magnitude of these changes will depend upon the material that constitutes each part, the radial dimensions of each part, and the radial reference point (r_r) of each part (usually the inner or outer surface.)

It is often possible to accurately model sections of a rotor as composite cylinders, using the analytical solutions of the linear elastic, open ended, thick wall cylinder, experiencing internal and external pressure. Equation 2.4 describes the radial deformation of a thick walled cylinder, which is exposed to an internal and/or external pressure (4).

$$u = \frac{r_r}{E(r_o^2 - r_i^2)}\left[(1-\nu)(p_i r_i^2 - p_o r_o^2) + \frac{(1+\nu) r_i^2 r_o^2}{r_r^2}(p_i - p_o)\right]$$

Equation 2.4: Radial Deformation in a Thick Wall Cylinder, Due to an Internal and External Pressure

It is important to know the state of stress in the rotor due to the pressures that may be exerted on certain parts, which may be the result of the interference fit that exists between two concentric axisymmetric members. Similar to the stress generated by the rotating body, uniaxial equivalent stress which is due to an interference fit can be computed using the components acting in the radial and circumferential directions (it is assumed that the cylinder is open-ended.) Radial and circumferential stress in cylinders which are

exposed to internal and external pressure are defined by Equations 2.5 and 2.6 (4).

$$\sigma_r = \frac{p_i r_i^2 - p_o r_o^2}{r_o^2 - r_i^2} - \frac{r_i^2 r_o^2}{r_r^2 (r_o^2 - r_i^2)} (p_i - p_o)$$

Equation 2.5: Radial Stress in a Thick Wall Cylinder, Due to an Internal and External Pressure

$$\sigma_\theta = \frac{p_i r_i^2 - p_o r_o^2}{r_o^2 - r_i^2} + \frac{r_i^2 r_o^2}{r_r^2 (r_o^2 - r_i^2)} (p_i - p_o)$$

Equation 2.6: Circumferential Stress in a Thick Wall Cylinder, Due to an Internal and External Pressure

Once again, similar to the stress in a rotating body, it is possible to use the values computed using Equations 2.5 and 2.6 with the applicable combined stress criteria, in the development of the uniaxial equivalent stress at the reference radius (r_r). It is noteworthy that Equations 2.1 through 2.6 do not include thermal effects. If all of the parts are made of the same material, and there are no temperature gradients in the rotor, the uniaxial equivalent stress will not change (5). Only the strain will be affected by thermal effects in that case. Neither the constant temperature distribution nor the single material assumption is necessarily valid in any particular case. The validity of each assumption will vary with each system.

2.3 Remarks

The importance of the analytical equations presented in this chapter is three-fold. First, they are tools that can be used to confirm FEA modelling accuracy. When analyzing complex rotor configurations, it is often possible to apply these equations to certain portions of the rotor in order to confirm proper trends within the FEA.

Second, it will be seen in Chapter Five that these equations can be used to accurately compute the critical radial dimensions of relatively complex rotor configurations. This reduces the time and computing power required of multiple FEA formulations (for various rotor operating conditions.) If the rotor to be analyzed is of a very simple axisymmetric geometry (such as a disk), then a FEA formulation is not required. This would imply that FEA may not be needed at all (in special cases.)

And finally, description of a mechanical system using two completely different mathematical methods (numerical and analytical) which produce similar results, reflects responsible engineering practice.

The tools required to analytically compute radial deformation characteristics in linear elastic, axisymmetric rotors have been presented. It is assumed that the reader is familiar with FEA, therefore the specific tasks of modelling and configuring data for computation using FEA are not

discussed. Application of the methods presented can be found in Chapter Five. For additional information concerning the analytical topics discussed in this chapter, the reader is referred to (3, 4, 5).

Chapter 3

MODAL ANALYSIS

The central concepts of this document, upon which all other dynamic system calculations are based, are the natural frequencies and mode shapes of the subject structure, which consists of a geometrically axisymmetric rotor and its elastic supports (located adjacent to the bearings). During normal operation, this rotor will spin about the bearing axis within a speed range of 15,000 to 30,000 RPM. During start-up and shut-down the system will also pass through the 0 to 15,000 RPM speed range. Small rotor imbalances will result in dynamic excitation forces in the spinning rotor.

It is assumed that the system behaves in a linear fashion throughout the normal operating speed range. Natural frequencies and mode shapes are calculated using the homogeneous form of the differential equations that describe the motion of the system. Then a prediction is made of the forced response of the system due to the imbalance force and moment and an estimate of the structural damping in the system.

Before beginning the modal analysis, it is important to determine whether or not the rotor being analyzed can be considered to be rigid with respect to bending, as rotor bending is a potential mode shape. If the rotor is not

essentially rigid, then the system dynamic properties of mass and support stiffness must be treated as distributed, rather than lumped properties. If the system dynamic properties are treated as distributed, then solution may require numerical techniques, because the differential equations of motion become non-linear.

For this analysis, the determination of rigidity is based on the frequency of the first rotor bending mode, assuming the rotor is supported rigidly. In other words, if the first rotor bending mode frequency is sufficiently high, then it is unlikely that any forcing function acting on the system will cause resonance at that frequency. Resulting stress (and strain) which is due to bending will be small, therefore the rotor is considered to be rigid with respect to bending.

The rigid body determination allows simplification of the analytical modal analysis into a two-degree-of-freedom, spring-mass (2 DOF) system. If the rotor were symmetrically supported about its mass center and non-rotating, the modes could be described relative to the rotor mass center as pure translation and pure wobble (see Figure 3.1). These modes could also be defined relative to transverse deflection at each rotor support, but this representation would not be convenient. Since the rotor is not necessarily symmetrically supported the two modes are coupled (unless the rotor is not rotating). It is therefore more precise to describe the modes

as predominantly translation, and predominantly wobble. This characteristic becomes obvious when the system eigenvectors are computed (see Section 3.3). In the interest of document readability, these modes of oscillation will subsequently be referred to simply as translation and wobble.

Gyroscopic effects produce various degrees of coupling between modes in different rotor systems. Depending on the rotor mass distribution and angular velocity, gyroscopic stiffening can significantly affect the system dynamics. Gyroscopic effects are well known and exploited in a variety of mechanical systems. The mathematical equation which describes this phenomenon will be developed in Section 3.2.

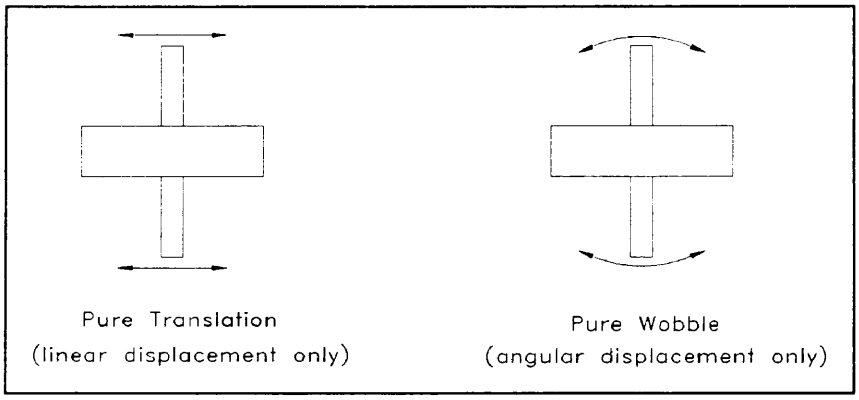

Figure 3.1: Modal Description

3.1 Natural Frequency Calculations

Natural frequencies exist in all electrical and mechanical systems, and their effect on this machine cannot be neglected. For example in an electrical system, Amplitude

Modulated (AM) radio wave reception is based on the superposition of a radio wave (having a specific frequency), upon the resonant frequency of an inductance/capacitance (LC) circuit. This type of system depends on the presence of a natural frequency for its normal operation.

The prediction of the natural frequencies (eigenvalues) and associated mode shapes (eigenvectors) is the first step in any vibration analysis. In the case of rotating machinery it is typical for a forcing function to be caused by rotor mass eccentricity (imbalance). This leads directly to the observation that a major, ever-present forcing function found in rotating machinery has a frequency equal to the spin velocity of the rotor. If the frequency of this forcing function is in the neighborhood of a system natural frequency, it will significantly influence the system response. The result will be excessive rotor vibrations with associated large dynamic support reaction forces and stresses, mechanical noise, decreased bearing life, etc. It is therefore important to ensure that no natural frequencies exist within the normal operating speed range of the rotor system. These negative effects can be predicted subject to the accuracy of the damping present in the system.

3.1.1: Numerical Techniques

In theory, mechanical systems are capable of exhibiting

an infinite number of modes, or degrees of freedom. However, if the mode is not excited by some forcing function, the system will not be affected. It is useful (for reasons which were discussed previously) to apply numerical techniques to determine the system resonant characteristics which are the result of rotor flexibility.

If the rotor has a constant cross-section, an analytical solution can be applied to determine the frequencies of the bending modes which are the result of rotor flexibility (6). For a rotor which has a cross-section that is not constant, a more sophisticated method is required. There are a number of techniques available for determining the frequency of bending modes associated with rotors of complex geometry. This analysis uses the numerical techniques developed by Kim (7) to determine the first rotor bending mode frequency (or critical speed). Application of Kim's techniques allows treatment of system dynamic properties as distributed. Application of these techniques requires treatment of the rotor supports as rigid. In other words, it is assumed that all system compliance is distributed in the flexible rotor, and the rotor supports (i.e., bearings and supporting fixtures) are assumed to be infinitely stiff.

3.1.2: Analytical Techniques

The physical importance of the rigid body determination

is two-fold. If the shaft is determined to be rigid with respect to bending, it follows that there exists infinite spring rate associated with shaft flexibility. The system compliance can then be assumed to be concentrated in the rotor mounting supports (i.e., bearings or other support fixtures). Alternatively, the rigid body determination also allows treatment of the entire mass of the rotor as sprung (or lumped) mass. Since the natural frequency is then directly related to rotor support spring rate and rotor mass (and mass distribution), and these system properties can be measured, the system natural frequencies can be reliably computed. In other words, if the system can be considered to be linear, then closed-form analytical techniques can be used to identify resonant frequencies and mode shapes.

The most general natural frequency calculations of rigid, 2 DOF systems account for support asymmetry and gyroscopic stiffening. Support asymmetry implies that the rotor supports are of unequal spring rate and/or are unequally spaced from the rotor mass center. The following modal derivation is constructed parallel to one that can be found in a previous study (6), with the primary difference being that this analysis also includes the gyroscopic stiffening effect.

Mathematical development of the differential equations of motion, which describe the rotor dynamic response, begins with an accurate model. Figure 3.2 displays all of the factors

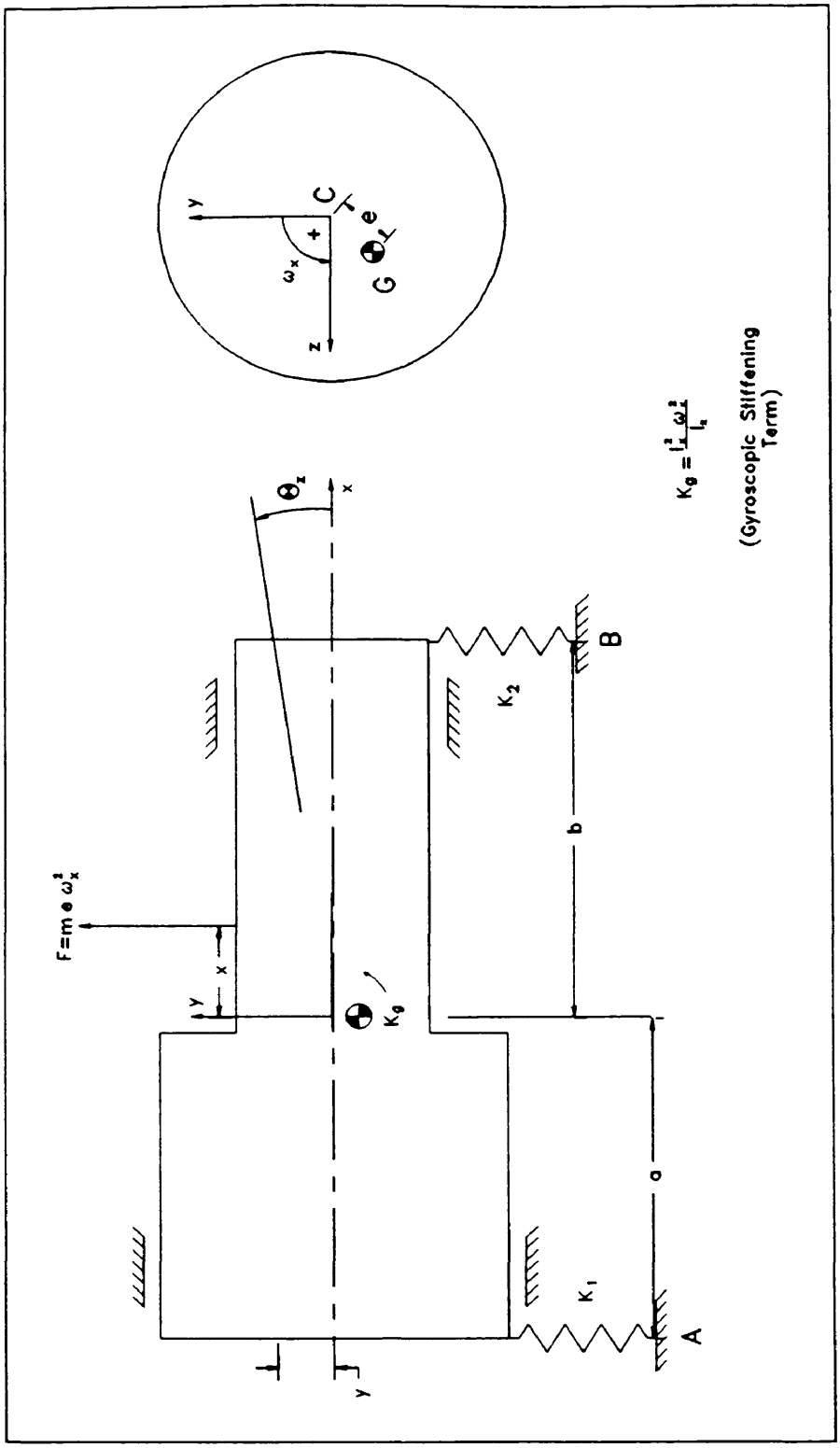

Figure 3.2: Rotor Model

that will be required to produce the equations of motion for this system. Radial ball bearings at locations "A" and "B" allow rotation about the "x" axis. "θ_z" and "y" are defined relative to the inertial reference frame described by the locus of points which forms a straight line between the rotor bearing centers (i.e., the axis of rotation).

If the rotor mass center (G) is not located on the axis of rotation (O), a condition known as **static imbalance** will exist (8). The degree of imbalance is denoted as a distance (e), which is also referred to as rotor eccentricity. When the rotor spins about the "x" axis with speed ω_x, an unbalance force equal to $me\omega_x^2$ results from this static imbalance. This force acts through the mass center (G) and is perpendicular to the axis of rotation ("x", Figure 3.2). Viewed from an inertial (fixed) reference frame this force appears to be sinusoidal, with amplitude of $me\omega_x^2$ and frequency of ω_x. The force generated by a static imbalance causes the rotor to vibrate in the translation mode of oscillation.

It is also possible that the rotor mass distribution creates a couple in the "x" "y" plane about the mass center, without generating a net centrifugal force (see Figure 3.2). This condition is known as a **couple imbalance** (8). It is possible to represent this force and couple as an equivalent force ($me\omega^2$) acting at a distance (x) from the axial position of the rotor mass center. Although it is not actually a free-

body diagram, by referencing Figure 3.2 it can be determined that the summation of forces in the "y" direction yields Equation 3.1.

$$me\omega_x^2 = m\ddot{y} + K_1(y-a\theta_z) + K_2(y+b\theta_z)$$

Equation 3.1: Summation of Forces

Inspection of Figure 3.2 reveals that the summation of moments about the mass center yields Equation 3.2.

$$xme\omega_x^2 = I_z\ddot{\theta}_z - K_1a(y-a\theta_z) + K_2b(y+b\theta_z) + \left(\frac{I_x^2\omega_x^2}{I_z}\right)\theta_z$$

Equation 3.2: Summation of Moments

The last group of terms in Equation 3.2 represents the gyroscopic stiffening phenomenon. This effect will be discussed in detail in Section 3.2. By regrouping terms, it is possible to display these two simultaneous differential equations in matrix form as:

$$\begin{bmatrix} m & 0 \\ 0 & I_z \end{bmatrix}\begin{Bmatrix} \ddot{y} \\ \ddot{\theta}_z \end{Bmatrix} + \begin{bmatrix} (K_1+K_2) & (K_2b-K_1a) \\ (K_2b-K_1a) & \left(K_2b^2+K_1a^2+\frac{I_x^2\omega_x^2}{I_z}\right) \end{bmatrix}\begin{Bmatrix} y \\ \theta_z \end{Bmatrix} = \begin{Bmatrix} me\omega_x^2 \\ xme\omega_x^2 \end{Bmatrix}$$

Equation 3.3

It is commonly accepted to analyze vibration problems using the mathematics which support the classic characteristic

value or eigenvalue problem. This approach is based on the observation that each mode of oscillation can be described as simple and harmonic. The resultant waveform may not appear to be simple, but each component of the waveform will be. The general form of the classic eigenvalue problem is demonstrated in Equation 3.4. The derivation of Equation 3.4 is not included in this document, however comprehensive formulations can be found in the literature (6).

$$[M^{-1}K - \lambda I] = 0$$

Equation 3.4

In Equation 3.4, $[M]^{-1}$ is the inverse mass matrix, [K] is the stiffness matrix, λ is the natural frequency squared, and [I] is the identity matrix. In Equation 3.4 the forcing functions are set equal to zero since the system natural frequencies are completely defined by the inertial and stiffness properties of the system (if damping is neglected).

From Equation 3.3, it can be seen that the mass and stiffness matrices are:

$$[M] = \begin{bmatrix} m & 0 \\ 0 & I_z \end{bmatrix}$$

Equation 3.5: Mass Matrix

$$[K] = \begin{bmatrix} (K_1+K_2) & (K_2b-K_1a) \\ (K_2b-K_1a) & \left(K_2b^2+K_1a^2+\frac{I_x^2\omega_x^2}{I_z}\right) \end{bmatrix}$$

Equation 3.6: Stiffness Matrix

It is somewhat curious that mass moment of inertia (I_x and I_z) and angular velocity terms are present in the stiffness matrix. Once again, that combination of terms represents the gyroscopic stiffening phenomenon.

The next step in this process is mass matrix inversion. It is noteworthy that the differential equations of motion were developed such that the mass matrix consists only of diagonal terms. This condition is referred to as **dynamic decoupling** (6). By this selection of coordinate systems, the task of mass matrix inversion has been simplified. The inverse mass matrix is displayed in Equation 3.7.

$$[M]^{-1} = \begin{bmatrix} \frac{1}{m} & 0 \\ 0 & \frac{1}{I_z} \end{bmatrix}$$

Equation 3.7: Inverse Mass Matrix

The dynamic matrix, which describes the dynamic properties of the system, is generated by multiplying the inverse mass matrix with the stiffness matrix.

$$[M]^{-1}[K] = \begin{bmatrix} \left(\frac{K_1+K_2}{m}\right) & \left(\frac{K_2b-K_1a}{m}\right) \\ \left(\frac{K_2b-K_1a}{I_z}\right) & \left(\frac{K_2b^2}{I_z}+\frac{K_1a^2}{I_z}+\frac{I_x^2\omega_x^2}{I_z^2}\right) \end{bmatrix}$$

Equation 3.8: Dynamic Matrix

Next, λ is subtracted from each of the diagonal terms. Mathematically, this is accomplished by subtracting the product of λ and the identity matrix, from the dynamic matrix (Equation 3.8). Since the matrices are now in the form of Equation 3.4, determinant computation is necessary in order to produce the characteristic equation.

$$|D| = \begin{vmatrix} \left(\frac{K_1+K_2}{m}\right)-\lambda & \left(\frac{K_2b-K_1a}{m}\right) \\ \left(\frac{K_2b-K_1a}{I_z}\right) & \left(\frac{K_2b^2}{I_z}+\frac{K_1a^2}{I_z}+\frac{I_x^2\omega_x^2}{I_z^2}\right)-\lambda \end{vmatrix} = 0$$

Equation 3.9

The characteristic equation is second order, corresponding to the two degrees of freedom. One of the frequencies represents the translation mode, and the other represents wobble. The characteristic equation is represented by Equation 3.10.

$$\lambda^2 - \left[\left(\frac{K_1+K_2}{m}\right)+\left(\frac{K_2b^2}{I_z}\right)+\left(\frac{K_1a^2}{I_z}\right)+\left(\frac{I_x^2\omega_x^2}{I_z^2}\right)\right]\lambda$$
$$+\left[\left(\frac{K_1+K_2}{m}\right)\left(\frac{K_2b^2}{I_z}+\frac{K_1a^2}{I_z}+\frac{I_x^2\omega_x^2}{I_z^2}\right)-\left(\frac{(K_2b-K_1a)^2}{I_zm}\right)\right] = 0$$

Equation 3.10: Characteristic Equation

Because the characteristic equation is second order, application of the quadratic equation to solve for the two roots is possible. Each root represents the square of its respective natural frequency (in units of radians per second.) It can be seen that the first and zero order coefficients in Equation 3.10 are positive definite. This implies that the roots of Equation 3.10 are also positive definite. Consistently, all examples investigated so far have produced positive and real roots.

Upon inspection of Equation 3.10, it can be seen that the natural frequencies are dependent on the rotor angular velocity. This dictates that an iterative process with respect to angular velocity is required in order to determine at what points the frequency of the forcing function is in the neighborhood of the natural frequencies. Recall that it is in the neighborhood of the natural frequency, where the forcing function most significantly influences the system response. This speed dependence of the natural frequencies physically means that as the rotor angular velocity increases, so will

the natural frequencies. Although the numerical value of the natural frequencies themselves are of great interest, the magnification factors and phase angles associated with rotor spin speeds (i.e., forcing function frequencies) near each natural frequency will be indispensable in the kinetic analysis. As it will be seen in Sections 3.4 and 3.5, computations of these phenomena are based on the ratio of the forcing function frequency to the natural frequency (frequency ratio).

Because the natural frequency is changing as a function of rotor angular velocity, the magnification factors and phase angles might exhibit non-standard characteristics. This is because the natural frequencies are dependant on the rotor operational speed. As a result, computations of magnification factor and phase angle will reflect a non-linear change in frequency ratio.

It is noteworthy that damping has been neglected in this derivation. The damped natural frequencies can be computed using the equation:

$$\omega_d = \omega_n\sqrt{1-\zeta^2}$$

Equation 3.11: Damped Natural Frequency

Since the rotor is assumed to be rigid it follows that, similar to spring rate, any damping observed in the system will be concentrated in the bearings or other support fix-

tures. Equation 3.11 results in a complex value for over-damped systems (damping ratio greater than 1.0). However, as it will be seen in Chapter Five, the damping ratio of this system is small, and therefore the damped natural frequency will be approximately equal to the undamped natural frequency.

3.2 Gyroscopic Stiffening

Anyone who has ridden a bicycle or played with a toy top has observed the phenomena associated with a gyroscope. However, the mathematical description of these phenomena are not necessarily obvious. Numerous derivations of gyroscopic stiffening can be found in the literature (9,10). Gyroscopic stiffening describes the resistance to angular displacement of the axis of rotation of a gyroscopic element. The following derivation is intended to enhance the presentations found in the references, rather than replace them. Please refer to Figure 3.3 for this derivation.

In the dynamic analysis of the gyroscopic element, it is useful to employ the same axis systems as those found in Figure 3.2. That is, the inertial reference frame, described by (X, Y, Z) is fixed in space. The non-inertial reference frame described by (X', Y', Z') is rotating with the rotor, at the rotor spin velocity (ω_x). This axis system does not violate Newton's laws because the angles are defined relative to the inertial reference frame.

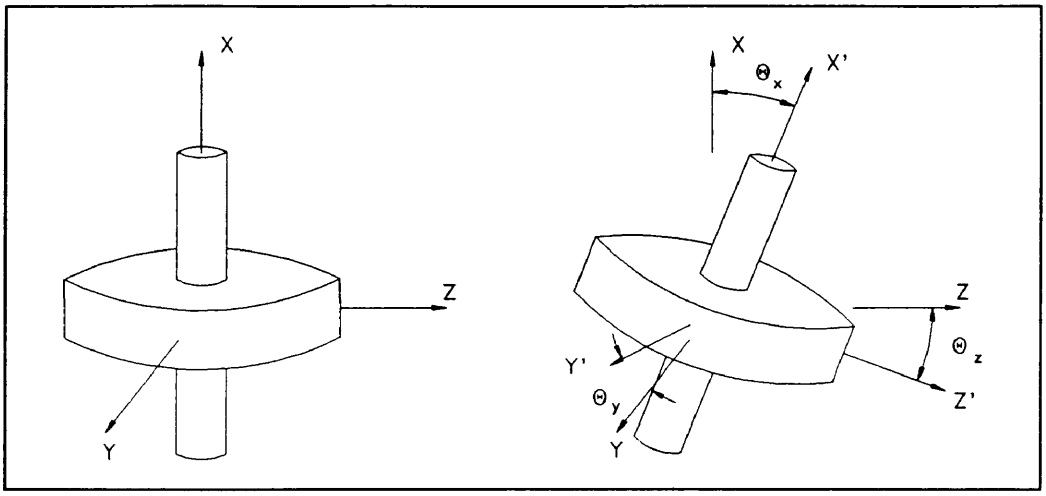

Figure 3.3: Axis System of
Gyroscopic Element

It is also important to note the assumptions made in this derivation:

a. Angular velocity, and therefore angular momentum, about the "X'" axis is constant. Since the small angle assumption is also made (Assumption "d") angular momentum about the "X" axis is also constant.

b. Torque (including friction) about the "X'" (and "X") axis is equal to zero.

c. The gyroscopic element has sufficient freedom to allow unrestrained precession.

d. The angle of deflection (θ_x) between the "desired" axis (X) and the "actual" axis (X') of rotation is small.

e. The torque generated by gravitational force is significantly smaller than the torque generated by the gyroscopic effect.

The theory behind the gyroscope rests upon the theorem of mechanics that the time rate of change of the angular momentum vector equals the applied torque vector (9). Since the

magnitude of angular momentum is constant (Assumption "a"), it must be the direction of the vector which describes the angular momentum that changes (note that acceleration need not necessarily reflect a change in speed--it may be the result of a change in direction.) If a torque is applied about the "Z" axis, the gyroscopic element will precess in the "Y" direction. Since the applied torque is equal to the time rate change of angular momentum, the torque is applied about the "Z" axis and angular momentum about the "X" (spin) axis is constant, it must be that the resultant precessional velocity is about the "Y" axis (the magnitude of the spin angular velocity does not change- only the direction of the vector changes). The mathematical representation of this phenomenon is:

$$T_z = I_x \omega_x \left(\frac{d\theta_y}{dt} \right)$$

Equation 3.12

Newton's second law of motion as it applies to rotation can be written as:

$$T_z = I_z \left(\frac{d^2\theta_z}{dt^2} \right)$$

Equation 3.13

If the gyroscopic element is in equilibrium, then the sum of moments about the "z" axis at the mass center is equal to

zero.

$$\sum M_z = I_z\left(\frac{d^2\theta_z}{dt^2}\right) - I_x\omega_x\left(\frac{d\theta_y}{dt}\right) = 0$$

Equation 3.14

In a subtle way, Assumption "e" has been applied to the development of Equation 3.14. If the torque caused by gravity were significant, it would be displayed on the right hand side of Equation 3.14. However, if that were true, it is also likely that the small angle assumption would no longer be valid. Integration of the time dependent terms in Equation 3.14 yields Equation 3.15.

$$\frac{d\theta_z}{dt} = \left(\frac{I_x\omega_x}{I_z}\right)\theta_y$$

Equation 3.15

Referring back to Figure 3.2 it can be seen that the springs at points "A" and "B" do restrict precession of the rotor. However, these boundary conditions have already been accounted for in Section 3.1. For this portion of the derivation the effect of those springs has been neglected (Assumption "c"). Since it is assumed that precession of the element is unrestrained, the system boundary conditions produce a constant of integration that is equal to zero. The left hand side of Equation 3.15 represents the angular velocity of precession of the gyroscopic element, which

results from a steady state angular displacement of the principal centroidal axis (10). Once again note that Equation 3.15 results from the equilibrium condition of the gyroscopic element. Now if a torque is applied by say, a couple imbalance within the element, or by a static imbalance in an asymmetrically supported rotor, the system will resist that torque, as its equilibrium condition is precession described by Equation 3.15. The resistance of the gyroscopic element to an angular change of the axis of rotation caused by an applied torque is described by Equation 3.16 (9,10).

$$T_z = I_z\left(\frac{d^2\theta_z}{dt^2}\right) + I_x\omega_x\left(\frac{d\theta_z}{dt}\right)$$

Equation 3.16

The first term on the right hand side of Equation 3.16 is identical to Equation 3.13. It represents Newton's second law of motion applied to rotation. The second term is similar to Equation 3.12. It represents the resistance to angular displacement of the "X'" axis. In fact, a 90 degree phase angle separates θ_y and θ_z, which implies that the magnitudes of these angles are equal, although they are not concurrent. Taking this into account, and substituting Equation 3.12 into the second term on the right hand side of Equation 3.16 yields:

$$T_z = I_z\left(\frac{d^2\theta_z}{dt^2}\right) + \left(\frac{I_x^2\omega_x^2}{I_z}\right)\theta_z$$

Equation 3.17: Resistance of a Gyroscope to an Applied Moment

The first term in Equation 3.17 has been previously accounted for in the equations of motion developed in Section 3.1. This term is not a function of system spin velocity (about the "X" axis.) Therefore, it is not considered to be an actual gyroscopic term. It was included to account for all physical factors affecting the gyroscopic element. In order to avoid counting this inertial term twice, it is removed from this portion of the analysis, leaving only the gyroscopic stiffening term. Once again, it is noteworthy that Equation 3.17 is valid only if the angle of deflection is small. This resulting term, which is proportional to angular displacement, can be considered to be an effective torsional spring, and can be included as an angular stiffness in the equations of motion:

$$T_z = \left(\frac{I_x^2\omega_x^2}{I_z}\right)\theta_z$$

Equation 3.18: Steady State Gyroscopic Angular Stiffness

3.3 Eigenvector Calculations

Associated with each natural frequency is a set of

coordinates that describes displacement of the rotor principal centroidal axis, with respect to its axis of rotation. This set of coordinates is commonly referred to as the **eigenvector** or **mode shape**. Since this is a 2 DOF system with respect to radial deflection, the eigenvector will contain two coordinates. The first coordinate represents transverse deflection of the mass center away from the axis of rotation (translation.) The second coordinate represents angular displacement within the "x" "y" plane, of the rotor about its mass center (wobble) (see Figure 3.2).

There are several commonly accepted eigenvector representations. In this analysis, the first coordinate (translation) is always equal to 1.0. This represents a unit displacement of the mass center. The second coordinate (wobble) is calculated relative to the first coordinate. In eigenvector computations, it is only the natural frequency that is coincident with the rotor angular velocity that is important. Therefore, although the natural frequencies are computed as a function of angular velocity, eigenvectors are computed only once for each mode. The following is a derivation of the equation used for computing the system eigenvectors.

Begin with a slight variation of the dynamic matrix (Equation 3.8), and multiply it by the coordinate system vector. This product is set equal to zero in order to compute the relative displacement coordinates associated with the free

response of the system. If the magnitude of the excitation force and moment at resonance were known, it would be possible to compute the absolute displacement values. However, it is not important in the modal analysis to know these absolute displacements. Only the coordinates describing rotor deflection during free response of the system are required to differentiate between the modes.

$$\begin{bmatrix} \left(\frac{K_1+K_2}{m}\right)-\lambda & \left(\frac{K_2b-K_1a}{m}\right) \\ \left(\frac{K_2b-K_1a}{I_z}\right) & \left(\frac{K_2b^2}{I_z}+\frac{K_1a^2}{I_z}+\frac{I_x^2\omega_x^2}{I_z^2}\right)-\lambda \end{bmatrix} \begin{Bmatrix} y \\ \theta_z \end{Bmatrix} = \begin{Bmatrix} 0 \\ 0 \end{Bmatrix}$$

Equation 3.19

It can be seen in Equation 3.19 that there are two possible equations that will result. Either of these equations can be used for the eigenvector computation. Since the first equation requires less computational load, it was chosen for this analysis. It should be obvious that the term λ will already have been computed, as the square of the natural frequency for which the eigenvector is being computed. The product of the upper terms of the dynamic matrix and the coordinate system vector is:

$$\left(\frac{K_1+K_2}{m} - \lambda\right) y + \left(\frac{K_2b - K_1a}{m}\right) \theta_z = 0$$

Equation 3.20

Next it is useful to group the coordinates "y" and "θ" on one side of the equation, and the system characteristic terms on the other side. Remember that the "y" coordinate is set equal to unity for this analysis, and therefore the "θ" coordinate is computed relative to 1.0 (representing a unit displacement in the translation mode.) The resulting equation after regrouping is Equation 3.21.

$$\frac{\theta_z}{y} = \frac{-\left(\frac{K_1+K_2}{m} - \lambda\right)}{\left(\frac{K_2 b - K_1 a}{m}\right)}$$

Equation 3.21: Eigenvector Equation

Equation 3.21 is used to compute the eigenvector coordinate that describes the wobble characteristics at the resonant frequency. It is noteworthy that under certain conditions this equation is undefined. Specifically, if the rotor is symmetric about its mass center, the denominator will be zero. Physically, this means that there will be no component of vibration in the translation mode. The only mode of vibration present will be wobble.

3.4 Forced Vibration Magnification Factor

The magnification factor represents a ratio of the steady-state forced vibration amplitude to the static displacement that the system would experience if the forcing

load were applied to it slowly (6). Similar to phase angle, computations of magnification factor are also based on the frequency ratio and damping ratio. The equation which describes this phenomenon is:

$$\frac{|X|}{F_0/k} = \frac{1}{\sqrt{\left[1-\left(\frac{\omega}{\omega_n}\right)^2\right]^2 + \left[2\zeta\left(\frac{\omega}{\omega_n}\right)\right]^2}}$$

Equation 3.22: Magnification Factor

It is important at this time to state that variation of the system damping ratio will significantly affect the system magnification factor only in the neighborhood of the natural frequency. It is also important to realize that when the angular velocity is much greater than the natural frequency, the magnification factor is less than 1.0. It decreases asymptotically toward zero with increasing angular velocity. The importance of both of these topics will be made clear in Chapter Five.

3.5 Forced Vibration Phase Angle

The phase angle is defined as the angle of separation between the steady state displacement and the excitation force (6). Its importance to rotating machinery becomes obvious when the rotor angular velocity (i.e., the forcing function frequency) is greater than the natural frequency. This condition will cause the phase angle to approach 180 degrees.

Physically, this means that the rotor will tend to rotate about its mass center. In terms of centrifugal force, this is generally a desirable phenomenon. If the rotor is approximately rotating about its mass center, support reaction forces are approximately zero.

Phase angle is computed based on frequency ratio (which in this case is defined as the ratio of rotor angular velocity to the natural frequency), and the damping ratio of the system. The results of these computations will be used in the kinetic analysis which is presented in Chapter Four. The equation for phase angle is commonly recognized as:

$$\phi = \arctan\left[\frac{2\zeta\left(\frac{\omega}{\omega_n}\right)}{1-\left(\frac{\omega}{\omega_n}\right)^2}\right]$$

Equation 3.23: Phase Angle

3.6 Remarks

All of the applicable dynamic fundamentals have been presented for use in the kinetic analysis. The mathematical development of phase angle and magnification factor were not presented. For further study of those topics, the reader is referred to (6).

Chapter 4

KINETIC ANALYSIS

The previous chapters, in and of themselves, possess significant engineering design value. However, those concepts can be exploited to an even greater degree by incorporating them into an analysis of the forces which act on an unbalanced rotor. From another perspective, kinetic analysis of this unbalanced rotor would be incomplete and inadequate without employing the concepts covered in Chapters Two and Three.

This analysis includes steady-state centrifugal force calculations of statically unbalanced rotors, moments generated by couple unbalanced rotors, and rotor support reaction force characteristics (including dynamic effects, gyroscopic stiffening and compliance within the rotor supports). The physical relationships between these effects are so complex that it is not intuitively obvious how variation in each dynamic property will affect the system. However, using the fundamental equations which describe each effect, it is possible to numerically quantify the system kinetic characteristics. The result of the kinetic analysis is an operational profile of the rotor forced (or total) response.

The data generated using the algorithm developed in this analysis do not reflect a real-time event. Iterations are accomplished with respect to angular (spin) velocity.

Transient conditions are ignored for three reasons. First, this would require implementation of a dimension in time, within the calculations. That would not be a trivial task. Second, considering dynamic effects, the steady-state condition at the resonant frequency is the worst possible case. It is well known that if the resonant frequency is passed through "quickly", dynamic effects will not become fully developed. Finally, the rotor system is designed so that it will operate in a stable condition regardless of how quickly the resonant frequency is passed through. For these reasons, the steady-state analysis is the item of interest.

There are two possible states that this rotor can operate in. The first state is described by metal-to-metal contact between the rotor inner surface and the bearing outer race. The second state is described by physical separation between the rotor inner surface and bearing outer race. The interface between these parts, while the device is in this state, is provided by an elastic interface. In its present revision, this algorithm does not generate valid data during operation described as metal-to-metal contact. However, metal-to-metal contact will be a transient condition, and it is assumed that the system will not normally operate in this state. Valid data are generated throughout the normal operating speed range.

4.1 Lever Rule

In order to compute the centrifugal force generated by an unbalanced, compliantly supported, 2 DOF rotor, it is first necessary to know the radial deflection of the rotor mass center. This can be determined with knowledge of rotor support deflections an simple geometric relationship:

$$\Delta y_c = \left(\frac{(a \cdot \Delta y_b) + (b \cdot \Delta y_a)}{(a+b)} \right)$$

Equation 4.1: Lever Rule

Figure 4.1 is a graphic representation of the Lever Rule. The name "Lever Rule" was adopted because of the "lever-like" relationship that exists between the deflections at the rotor supports and the mass center. Equation 4.1 is based on the rigid rotor assumption. Because the rotor is rigid, a constant, linear relationship exists between each of the points which describes the rotor principal centroidal axis, regardless of operating conditions.

Since an iterative analytical process (with respect to rotor angular velocity) is used to find the steady-state rotor kinetic characteristics, rotor support deflections from the previous iteration are used to determine the centrifugal force for the present iteration. This is the only obvious method for analytically predicting the kinetic characteristics of the unbalanced rotor. No finite difference techniques are

employed in this analysis, so stability of calculations is not an issue. It is noteworthy that the rotor principal centroidal axis does not necessarily coincide with the axis of rotation. Determination of the radial position of the rotor mass center, with respect to the axis of rotation, is the primary problem to be solved in the kinetic analysis. The implications of this problem will be discussed in the following section.

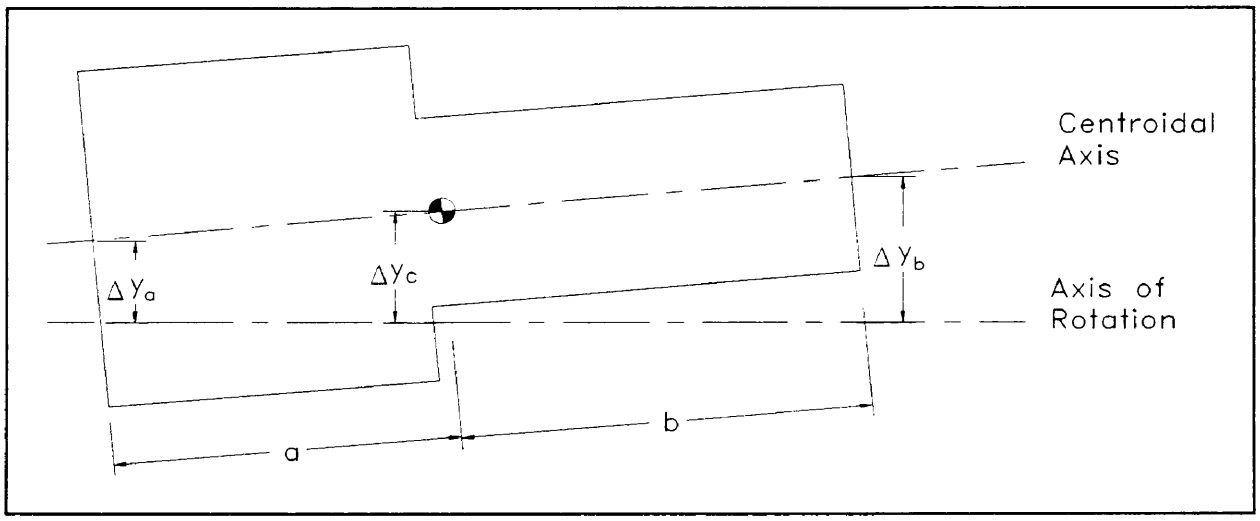

Figure 4.1: Graphic Representation of
The Lever Rule

4.2 Centrifugal Force

Centrifugal force acts on a rotating body in several different ways. In Chapter Two it was seen that the rotor deforms radially due to centrifugal force. In the kinetic analysis, centrifugal force also affects the rotor unbalanced

response. Figure 4.2 describes the radial position of the rotor mass center with respect to the axis of rotation, assuming the rotor supports are rigid. Note that since the rotor supports are assumed to be rigid, there are no dynamic effects represented in Figure 4.2.

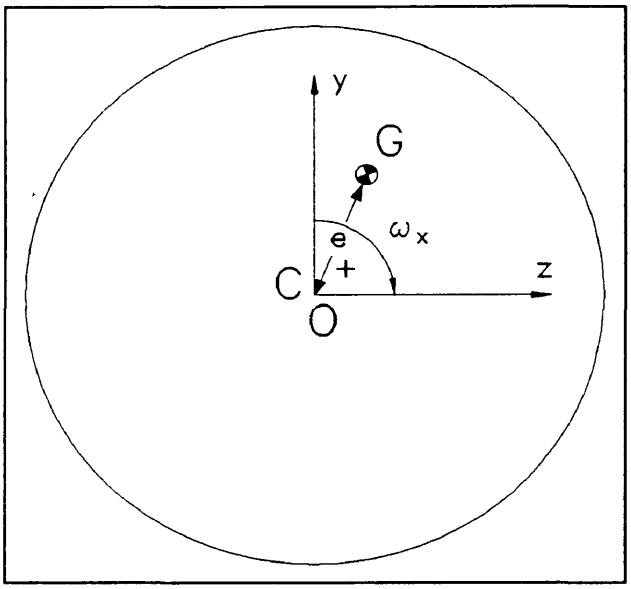

Figure 4.2: Eccentricity of Rigidly Supported, Rigid Rotor

In Figures 4.2 and 4.3, point "O" is the geometric bearing center. Point "C" is the point on the rotor principal centroidal axis, that is also in the plane of the rotor mass center (points "O" and "C" are co-located in Figure 4.2). Point "G" is the location of the rotor mass center, and "e" is the static eccentricity. In Figure 4.2, the rotor is constrained to rotation about point "O", while in Figure 4.3 the

rotor is allowed to displace, due to the compliance in the rotor supports. The primary difference between Figures 4.2 and 4.3 is that Figure 4.3 includes system dynamic effects.

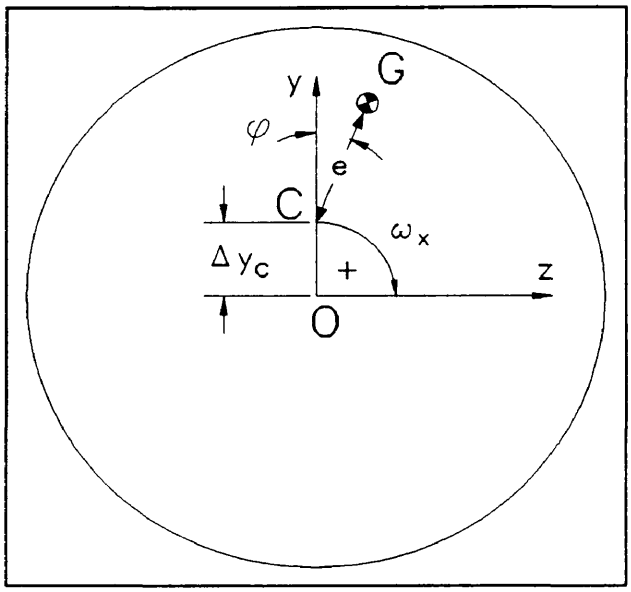

Figure 4.3: Eccentricity of Compliantly Supported, Rigid Rotor

The equation which describes the steady-state centrifugal force generated by eccentricity of the rigidly supported rotor presented in Figure 4.2 is:

$$F = me\omega_x^2$$

Equation 4.2: Force Generated by Rigidly Supported, Unbalanced Rigid Rotor

Equation 4.2 is still valid without the rigid rotor support assumption displayed in Figure 4.2, however the

distance separating the rotor mass center from the axis of rotation is no longer simply static eccentricity ("e"). Dynamic effects and rotor support compliance must also be considered in order to accurately define the total rotor eccentricity (e_{tot}).

The following computation of rotor eccentricity is similar to one found in a previous study (6), where the analysis of a rigidly supported, flexible rotor is developed. The following analysis is different because it assumes that the rotor is rigid, and accounts for compliance in the rotor supports only.

Calculation of the total rotor eccentricity begins with a two dimensional analysis of the rotor eccentricity, including compliance within the rotor supports and dynamic effects. As it was previously stated, deflection of the principal centroidal axis (which was computed on the previous iteration of the algorithm) is used with the Lever Rule to compute the distance described by OC (Δy_c) in Figure 4.3. This distance reflects the eccentricity resulting from compliance within the bearings or rotor support fixtures.

Since the rotor supports are compliant, there is a spring rate associated with each support. The natural frequency, and therefore phase angle, can be computed for this system (as described in Sections 3.1.2 and 3.5). The phase angle is represented in Figure 4.3 by the angle "ϕ". It can be seen in

Figure 4.3, that if the phase angle is approximately 180 degrees (corresponding to operation in the super-critical speed range with little damping), then the total eccentricity will be decreased significantly.

In order to compute the total eccentricity, it is useful to first compute the "Y" and "Z" components separately. In Figure 4.3 it can be seen that the "Y" component of eccentricity is defined as:

$$e_y = \Delta y_c + e \cdot \cos(\phi)$$

Equation 4.3: "Y" Component of Total Rotor Eccentricity

In Figure 4.3 it can also be seen that the "Z" component of eccentricity is defined as:

$$e_z = e \cdot \sin(\phi)$$

Equation 4.4: "Z" Component of Total Rotor Eccentricity

The resultant total rotor eccentricity can be found by computing the vector sum of these orthogonal components:

$$e_{tot} = \sqrt{e_y^2 + e_z^2}$$

Equation 4.5: Total Rotor Eccentricity

The result of Equation 4.5 (e_{tot}), is input into the eccentric term in Equation 4.2. The result of this process is the centrifugal force generated by a static imbalance in a rotor

which is mounted in compliant supports.

Although the centrifugal force has been computed, its real significance is how the rotor responds to the dynamic application of the force. In order to determine its effect, the centrifugal force must first be multiplied by the magnification factor which corresponds with the translation mode of oscillation (MF_t). (Note that the magnification factor is a scalar quantity.) Recall that a 2 DOF system will have two natural frequencies, and therefore two magnification factors.

$$F_{eff} = (MF_t)\, F$$

Equation 4.6: Effective Centrifugal Force

F_{eff} is the effective force that is transmitted through the rotor support fixtures (ie; bearings, etc). This is the central force of the kinetic analysis. Steady-state rotor support reaction forces and moments generated by couple imbalance are both based on the results of Equation 4.6.

4.3 Moments Generated by Centrifugal Force

Referring back to Figure 3.1, it can be seen that if the axial position of the imbalance is not located at the same axial position as the mass center, then a moment about the rotor mass center will be generated by the imbalance. The force will be F_{eff} (developed above). The moment arm will be X, representing the axial distance between the rotor centroid

and the location of the imbalance. Once again, it is the physical effect that this moment has on the system that is important to the kinetic characteristics. Therefore, the moment must be multiplied by the magnification factor that corresponds with the wobble mode of oscillation (MF_w). The effective moment that will cause wobble oscillation in the rotor is defined as:

$$M_{eff} = F_{eff} \; X \; (MF_w)$$

Equation 4.7: Effective Moment Due to Couple Imbalance

There are two interesting points that can be made concerning Equation 4.7. First, if the resonant frequency associated with the wobble mode is not numerically close to the resonant frequency associated with the translation mode of oscillation, there will be very little effective eccentric force generated (for use in the moment equation). The reason for the relatively small effective eccentric force is, if the frequency of the forcing function is not greater than about 60% or less than about 130% of the translational natural frequency, then the magnification factor will not be greater than about 1.5. Consequently, there will be a relatively small moment acting on the system.

Second, if a significant moment is generated, the system will oscillate in both the translation and wobble modes, at a

frequency equal to the rotor angular velocity. The fact that both of these forcing functions operate at the same frequency could make it difficult to discriminate between the effects of a static and a couple imbalance. This could complicate the task of rotor balancing.

4.4 Gyroscopic Stabilization

The fundamental dynamic equation which describes the concept of gyroscopic stiffening (3.18) was developed in Section 3.2. It is useful to begin this portion of the analysis by re-introducing Equation 3.18:

$$T_z = \left(\frac{I_x^2 \omega_x^2}{I_z} \right) \cdot \theta_z$$

Equation 4.8: Gyroscopic Stiffening Effect

Upon inspection of Equation 4.8, it can be seen that the effect of this phenomenon on the rotor kinetic characteristics is described as a resistance to angular displacement of the rotor spin axis ("X'" in Figure 3.3). Once again by making a small angle approximation, this resistance can be adequately modelled as proportional to angular displacement of the instantaneous spin axis, relative to the support bearing axis. It is therefore necessary to determine the angular displacement of the instantaneous spin axis (θ_z) that would exist if gyroscopic stiffening were not considered.

Determination of the angular deflection of the principal centroidal axis begins with a static model, including the centrifugal force and moment developed in Sections 4.2 and 4.3. It can be seen in Figure 4.4 that by summing forces in the "Y" direction, and moments about the mass center, that the rotor support reaction forces can be determined for any given eccentricity "e" and wobble angle "θ_z".

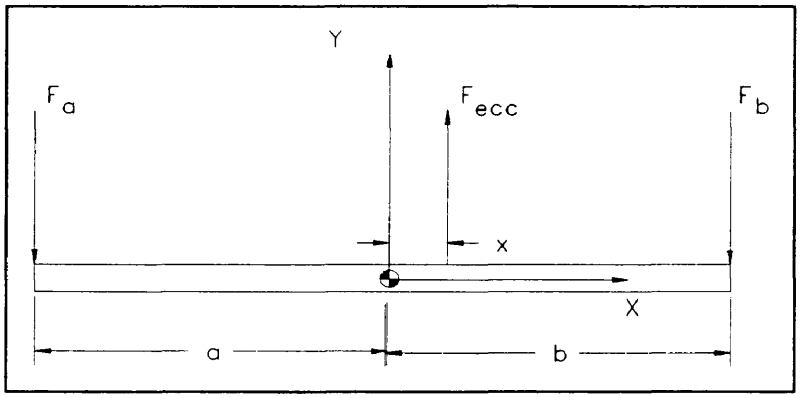

Figure 4.4: Free Body Diagram of Rotor

With knowledge of the force transmitted through each rotor support, and the spring rate of each rotor support, deflection of the principal centroidal axis at the axial position corresponding with each rotor support can be determined using Equation 4.9.

$$\Delta y = \frac{F_y}{k}$$

Equation 4.9: Deflection of a Compliant Rotor Support

In typical rotor systems, which are not fully unrestrained, a more complete deflection analysis is necessary. This is because, as stated in Chapter Two, if the bearing outer race is rotating with the rotor, then there will be a differential radial deformation rate between the rotor and the bearing. In addition, if the dimensions of the rotor are different at each bearing location, then the clearance that exists between the rotor and bearing will not be equal at each location. The result is that there are limits of rotor deflection which are defined by the radial clearance that exists between the bearing outer race and the inner surface of the rotor.

In a rotor of this configuration, it is assumed that the compliance will be concentrated in an elastic interface, which exhibits linear force-to-displacement characteristics, and is located in the clearance that exists between the bearing outer race and the inner surface of the rotor. There is also some compliance within the bearing, however the spring rate of the bearing is typically at least one order of magnitude greater than the spring rate of the device that is placed in the clearance region. Therefore, it is assumed that no deflection occurs within the bearing.

The previous statements reveal that there are limits of deflection that exist at each rotor support. The rotor deflection is limited by the radial clearance that exists

between the bearing and rotor inner surface at each support location. It was previously believed that there are 12 possible sets of boundary conditions that can be applied to this system. Figures 4.5a and 4.5b illustrate those possible boundary conditions. Calculations of support reaction forces in Chapter Five included all of these boundary conditions. It was subsequently determined that Cases 1, 2 (Figure 4.5a), 7 and 8 (Figure 4.5b) are invalid. This does not present a problem for this analysis because those particular cases can only arise when metal-to-metal contact is occurring between the bearing outer race and rotor inner surface (first state). It was previously stated that these calculations are not valid if metal-to-metal contact is occurring between these parts. However, in the normal operating speed range, this phenomenon will not be observed. One of Cases 3 to 6, or 9 to 12 will apply within the normal operating range.

After the rotor support deflections have been computed for the condition which does not include gyroscopic stiffening, the angle between the axis of rotation and the principal centroidal axis must be computed. Equation 4.10 analytically describes this angle:

$$\theta_z = \left(\frac{\Delta y_a - \Delta y_b}{a + b} \right)$$

Equation 4.10: Angle of Deflection of the Rotor Centroidal Axis, Neglecting Gyroscopic Stabilization

Equation 4.10 is a simple geometric relationship that assumes a small angular deflection of the centroidal axis. Figure 4.1 illustrates the basis of Equation 4.10. The angle θ_z is multiplied by the other values in Equation 4.8, to yield the resisting moment that is generated by the gyroscopic stiffening effect of the rotor. This moment is converted into an effective resisting force by dividing by the distance separating the rotor supports. The application of these resisting forces will tend to cause the principal centroidal axis to be parallel to the axis of rotation.

The logical nature of the possible boundary conditions defined by Figures 4.5a and 4.5b, lends itself nicely to digital manipulation of the conditions. In other words, "if-then" conditional statements can be easily implemented in a computer program to apply any of the possible boundary conditions that can occur during the operation of this rotor system.

4.5 Remarks

All of the concepts required for the kinetic analysis of this system have been presented. When producing a computer program to compute the kinetic characteristics of a rotor with this configuration, Newton's laws of motion must be satisfied. In other words, the sum of rotor support reaction forces must be equal to the effective centrifugal force generated by the

eccentric rotor. In addition, caution should be exercised when applying the boundary conditions described in Figures 4.5a and 4.5b.

It is once again noteworthy that if the elastic interface which exists between the rotor inner surface and bearing outer race is fully compressed, allowing the outer race and rotor to come into contact, this analysis is no longer valid. There are two reasons for this. First, if the elastic interface becomes fully compressed, then the rotor support stiffness is the stiffness of the bearing. Because of the large difference in stiffnesses of these materials, natural frequencies, and therefore dynamic response of the system will be significantly affected. The second reason is that boundary conditions 1,2,7 and 8 are not valid. These boundary conditions apply during the same operating speed range that has already been determined to be invalid (because of the bearing stiffness in natural frequency calculations).

A computer program has been developed to analyze a system of this configuration. Chapter Five consists of the application of theories presented in Chapters Two, Three and Four. Two specific rotor configurations and the results generated by these analytical techniques will demonstrate the proper application of these techniques, and the considerably different behavior that can be exhibited by radically different dynamic systems.

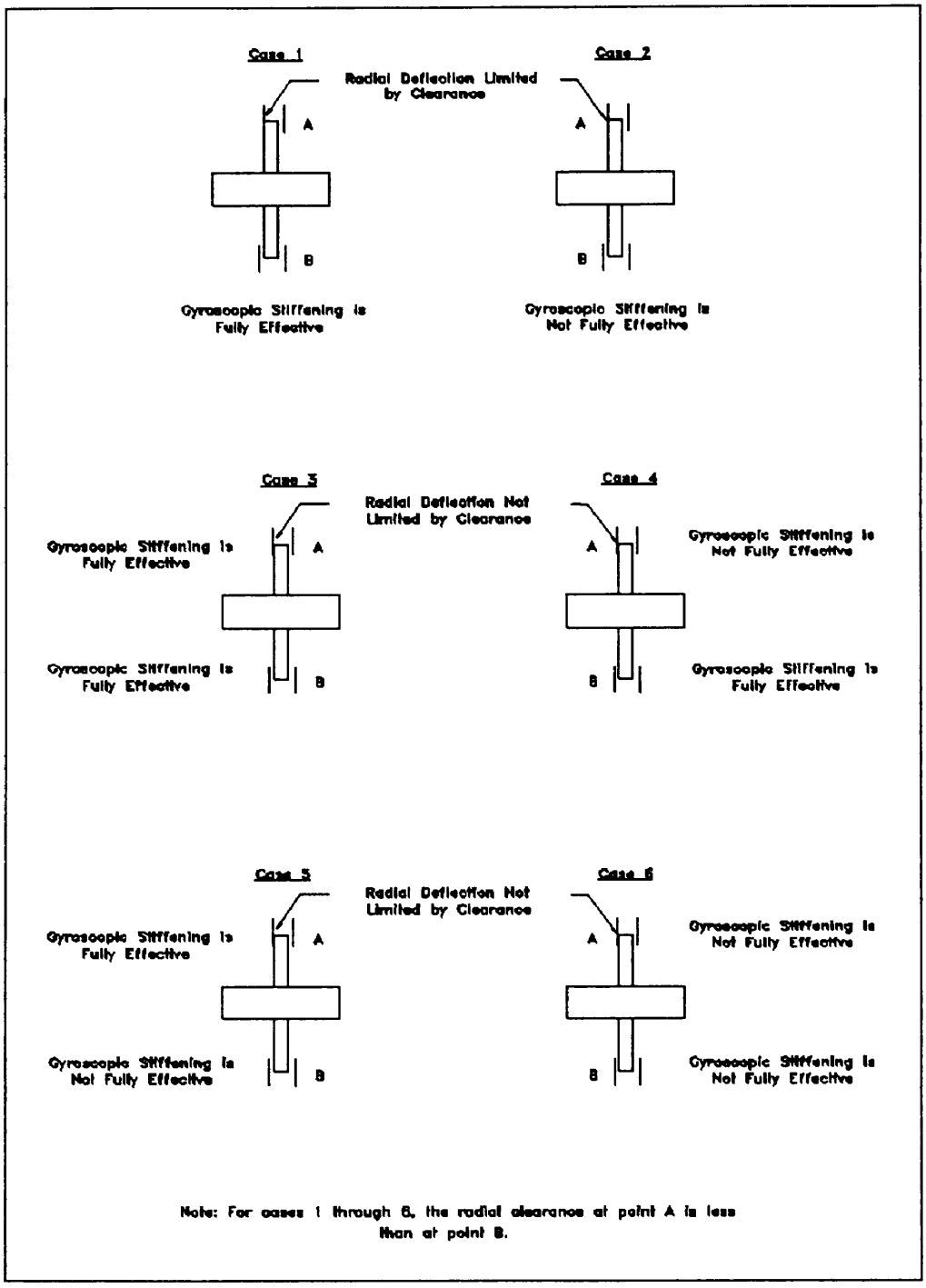

Figure 4.5a: Possible Boundary Conditions Applicable to the Compliantly Mounted, Rigid Rotor with Limited Deflection

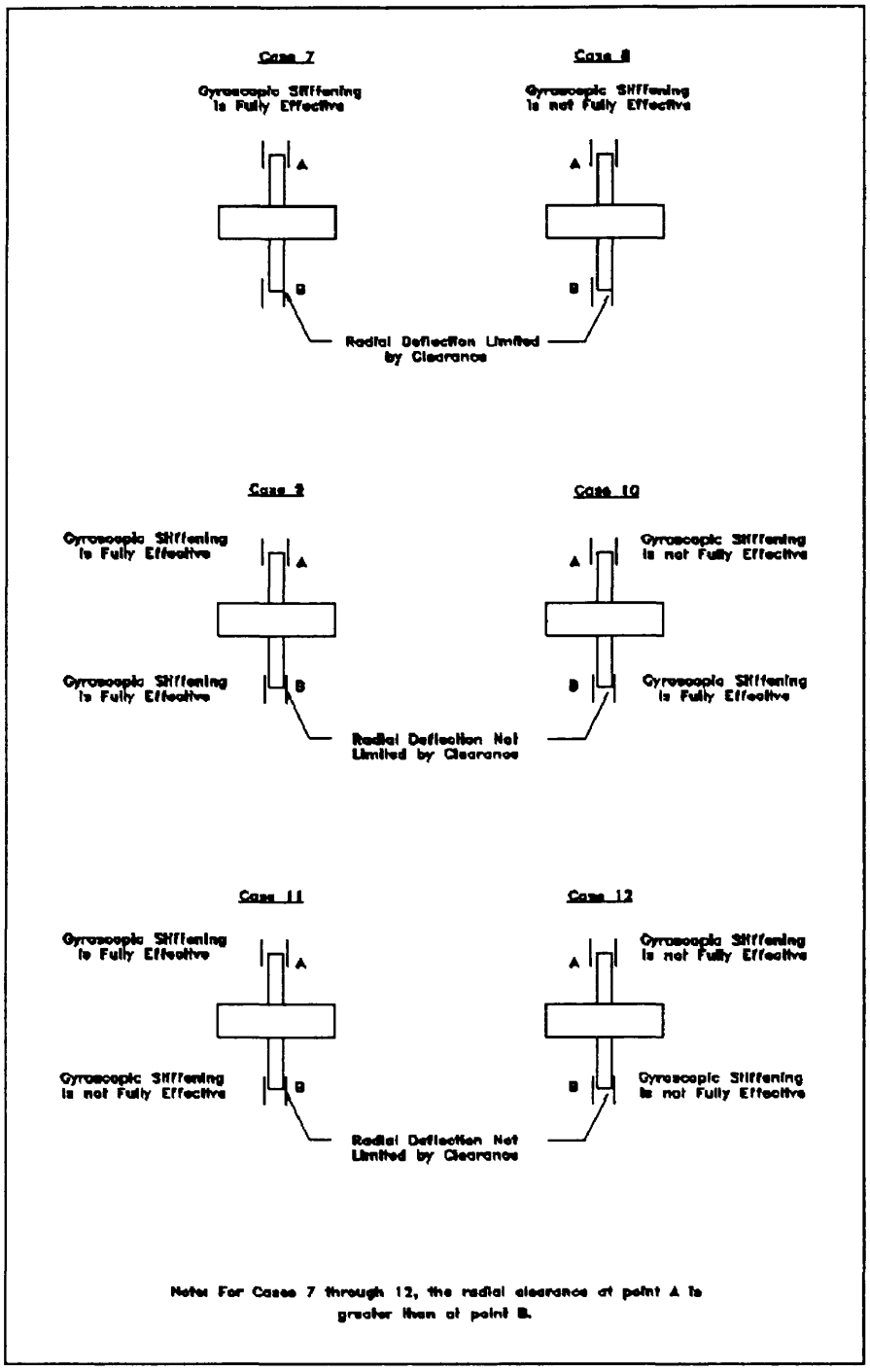

Figure 4.5b: Possible Boundary Conditions Applicable to the Compliantly Mounted, Rigid Rotor with Limited Deflection (cont.)

Chapter 5

APPLICATION OF THEORIES

The analytical techniques presented in Chapters Two, Three and Four have been integrated into a Fortran computer program (BIGPIC.FOR) that is capable of providing a comprehensive analysis of the given rotor configuration. In fact, it was for the particular rotors presented in this chapter, that this analysis was developed. It is noteworthy that certain information which is considered to be proprietary, has been omitted from this analysis. However, even without this information, a full appreciation of the presented techniques can be developed.

Two rotors are presented in this analysis, so that a comparison of dynamic characteristics can be made. Both will be subjected to the same operating requirements. Specifically, each will be capable of transitional speeds from 0 to 15,000 RPM, and continuous operational speeds from 15,000 to 30,000 RPM. The aspects that will be presented as evidence in support of proper analysis techniques are:

1. Radial deformation of the rotor and bearings.
2. Validity of the small angle approximation.
3. Speed dependence of natural frequencies.
4. Dynamic system factors (magnification factor and phase angle.)

5. Kinetic effects including:
   a. Centrifugal force generated by rotor eccentricity.
   b. Rotor support reaction forces.

6. Radial clearance between the rotor inner surface and bearing outer races including the eccentric force.

5.1 Rotor Configurations

Figure 5.1 is the cross-sectional view of the simplified first rotor configuration to be analyzed.

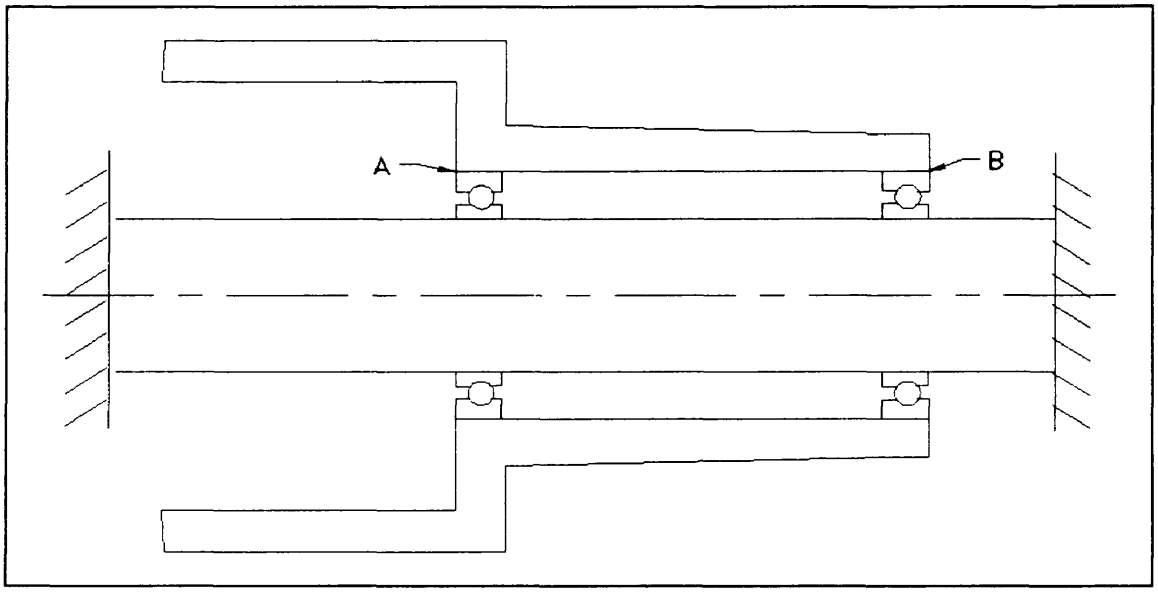

Figure 5.1: Simplified First Rotor

The dynamic properties of this rotor are as follows:

I_x = 0.163 in-lb-sec^2
I_z = 0.927 in-lb-sec^2
Wt = 16 lb
K_1 = 20,000 lb/in
K_2 = 20,000 lb/in
a = 1.09 in
b = 3.75 in

Both of the rotors under analysis are made of 4340 heat treated steel. It can be seen that in this rotor, the mass moment of inertia about the axis of rotation (I_x) is significantly smaller than I_z. By inspection of Equation 3.17, it can be predicted that this system will not benefit greatly from gyroscopic stabilization (compared to the second rotor). Statically, there is a line-to-line fit between the bearing outer race and the rotor inner surface at point "A". At point "B" there is a 0.0002 in. radial clearance in the static condition.

It has been predicted that this rotor will have approximately 0.08 oz-in. of imbalance, which will be concentrated near the rotor mass center. It has been found to be useful in this analysis to measure imbalance as the radial distance between the geometric bearing center and the rotor mass center, when the rotor is not rotating (see Figure 4.2). Although it is a non-standard representation, degree of imbalance will subsequently be reflected as a distance (i.e., 0.0003 in. eccentricity.) Considering the fact that the first rotor weighs 16 lbs., this 0.08 oz-in. imbalance corresponds with 0.0003 in. eccentricity.

Figure 5.2 is the cross-sectional view of the second simplified rotor configuration to be analyzed. By comparing Figures 5.1 and 5.2, it can be seen that these rotors are identical, except for the disk shaped flywheel which is

mounted on the second rotor. The dynamic properties of this rotor are as follows:

I_x = 3.19 in-lb-sec^2
I_z = 2.54 in-lb-sec^2
Wt = 53 lb
K_1 = 20,000 lb/in
K_2 = 20,000 lb/in
a = 2.02 in
b = 2.82 in

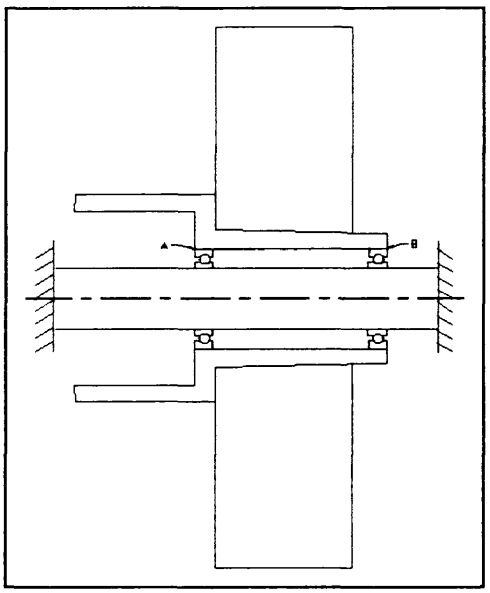

Figure 5.2: Simplified Second Rotor

Based on the relationship of the mass moments of inertia of this rotor (I_x and I_z), it can be predicted that this system will behave as a classic gyroscope. In fact, it will be seen that this system is significantly more stable than the first system. This rotor also has a line-to-line fit between the rotor inner surface and the bearing outer race at point "A".

At point "B" there is a 0.001 in. radial clearance between the bearing outer race and the rotor inner surface, at zero RPM.

It has been predicted that the eccentricity of this rotor will be 0.0003 in. until approximately 20,000 RPM. At that point, the eccentricity will increase linearly to 0.001 in. at 30,000 RPM. This eccentricity profile is referred to as **scheduled eccentricity.** It is theorized that this is due to the non-uniform expansion characteristics of the composite material flywheel. Since the composite flywheel is not homogeneous or isotropic, it is likely that the radial growth characteristics discussed in Chapter Two will not apply to this component. It is likely that the growth characteristics in the flywheel will not be described as axisymmetric either. If radial growth of the flywheel is a function of angular position around the flywheel, then the mass center of that component will change position as a function of angular velocity.

5.2 Radial Deformation

The state of stress and radial deformation of these rotors can be modelled as axisymmetric in three discrete sections, which allows application of the analytical solutions presented in Chapter Two. Assuming the rotor does not experience catastrophic failure, the only radial growth data required for this analysis are at points "A" and "B" (between

the inner surface of the rotor and the bearing outer races.)

The discrete rotor sections are displayed in Figure 5.3. The first section is described by the cylindrically shaped rotor material that connects the two rotor support fixtures. The second section is described as disk-like, and is adjacent to the rotor support at point "A". The third section is also cylindrical. Its purpose is to contain the permanent magnets necessary for operation of an electric motor/generator. The electric motor/generator is responsible for the conversion between mechanical and electrical energy, as described in Chapter One.

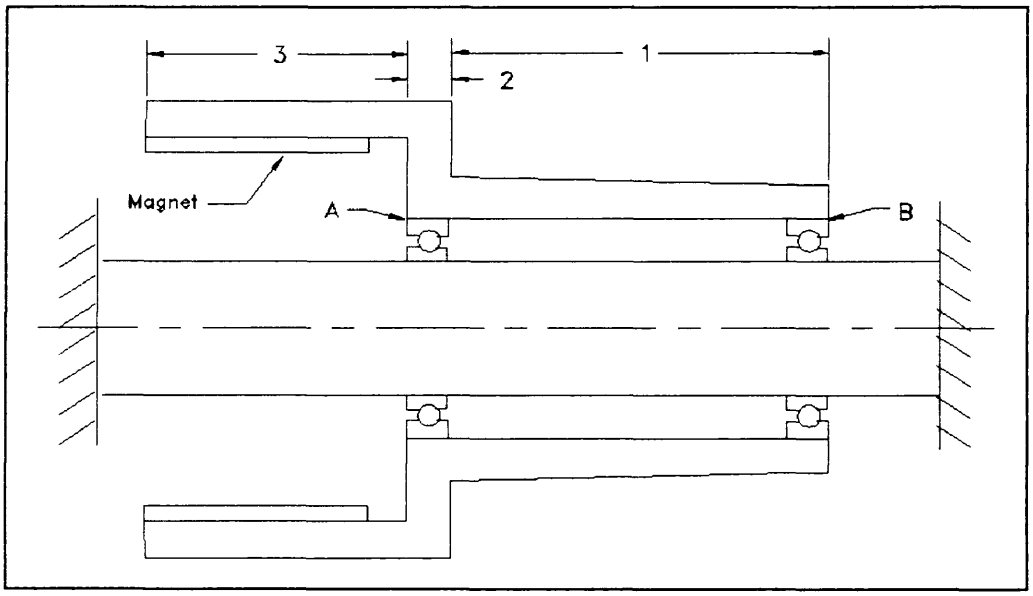

Figure 5.3: Discrete Rotor Sections

The third section is not truly axisymmetric because of

the discontinuous placement of six permanent magnets on the inside surface of the rotor. These magnets cover approximately 70% of the inner surface of the third rotor section. It will be seen later in this section that for purposes of this analysis, the third section can be adequately modelled as axisymmetric.

In order to determine the radial clearance between the bearing outer race and the rotor inner surface (which is required prior to accurate prediction of bearing reaction forces), it is first necessary to compute the radial deformation of the bearing outer race. Two effects will cause deformation in the outer race-- the angular velocity of the race itself, and the centrifugal force of the balls against the inner surface of the outer race. The effect caused by the balls can be modelled as an internal pressure which is proportional to the mass and radius (i.e., distance from the axis of rotation) of the balls, and angular velocity squared. Equations 2.1 and 2.4 can then be used to determine the radial deformation that occurs at the outer surface of the bearing outer race.

Similar to the centrifugal force of the balls against the bearing outer race, the magnets (which are located in section three) exert force on the inner surface of the rotor. This force can also be modelled as an internal pressure, distributed evenly on the inner surface of the third rotor section. It

was found that by modelling the magnets as axisymmetric, the uniaxial equivalent stress on the inner surface of the third rotor section will be 78 ksi. at 30,000 RPM. Using the axisymmetric simplification implies that the pressure caused by the centrifugal acceleration of the magnets is uniform on the inner surface of the rotor. Figure 5.4 reveals that an accurate stress distribution within the vicinity of the magnets will not be generated using the internal pressure simplification. In this case, FEA has been used to accurately describe the stress distribution in that region.

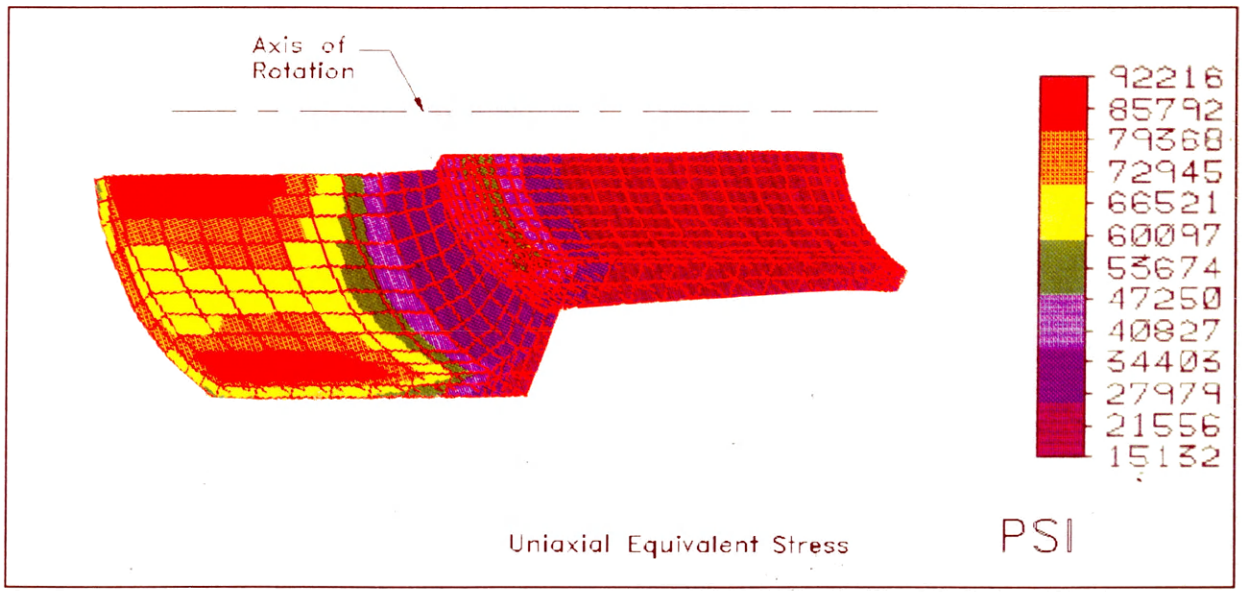

Figure 5.4: FEA of 3-D Rotor Section
With Magnets, Rotating at 30,000 RPM

To generate the stress distribution found in Figure 5.4, the material elastic modulus was applied to the cross-

sectional nodes as a stiffness, to provide the boundary conditions necessary for the analysis. The octahedral shear stress criterion was used in the development of the uniaxial equivalent stress in Figures 5.4 through 5.6.

The sectional FEA model in Figure 5.4 was used instead of the entire rotor for two reasons. First, this model takes advantage of the periodic, radial symmetry of the part. This significantly reduces the required modelling effort and computing power. Although the rotor is not truly axisymmetric because of the magnets, it is possible to analyze a section of the rotor with one magnet. The stress distribution in the other radially symmetric sections will be exactly the same as in this one. The second reason for using this model is that it is easier to view the stress distribution in the part. If the complete rotor were analyzed, it would be difficult to view the stress distribution in the rotor cross-section.

Figure 5.5 presents an axisymmetric view of the stress in the rotor if the centrifugal effects of the magnets were modelled as an internal pressure (axisymmetric simplification). Note that very good correlation is realized by comparing the uniaxial equivalent stress near the free end of the rotor (in section three) with the analytical solution presented earlier in this section (78 ksi at the inner surface).

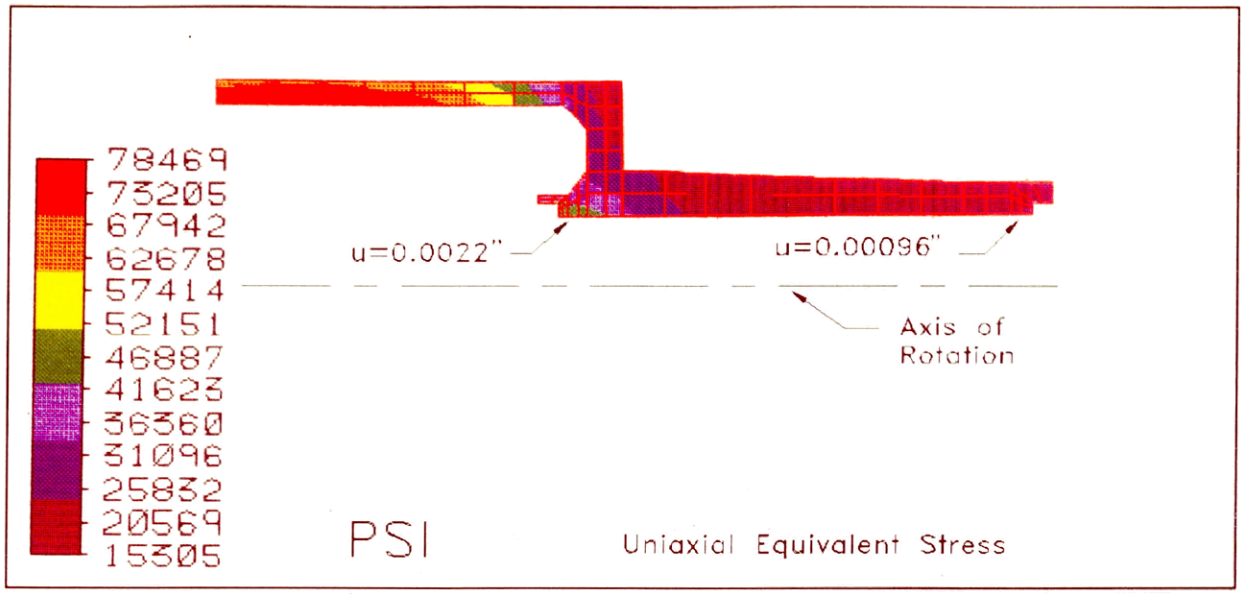

Figure 5.5: FEA of Axisymmetric Rotor With Magnets, Rotating at 30,000 RPM

Figure 5.6 is the same view, only without the effects of the magnet. The radial deformations at points "A" and "B", as well as the uniaxial equivalent stresses presented in Figures 5.5 and 5.6, were generated using the Algor software.

By comparing Figures 5.5 and 5.6, it can be seen that in terms of radial deformation in the rotor material which is adjacent to the bearing at point "A", it does not matter if the magnets are modelled at all. In fact, using the dimensions of section two in Equation 2.1, it was found that the radial deformation in this region will be 0.0023 in. at 30,000 RPM. Comparing this value with that found in Figure 5.5 (0.0022 in.), it can be seen that the difference is 0.0001 in. Two conclusions can be drawn from this comparison. First, it

appears as if the FEA model has been properly developed. The mesh density is adequate and the boundary conditions have been applied correctly. Second, sections one and three (including magnets) have negligible effect on the radial deformation in the rotor adjacent to the bearing at point "A".

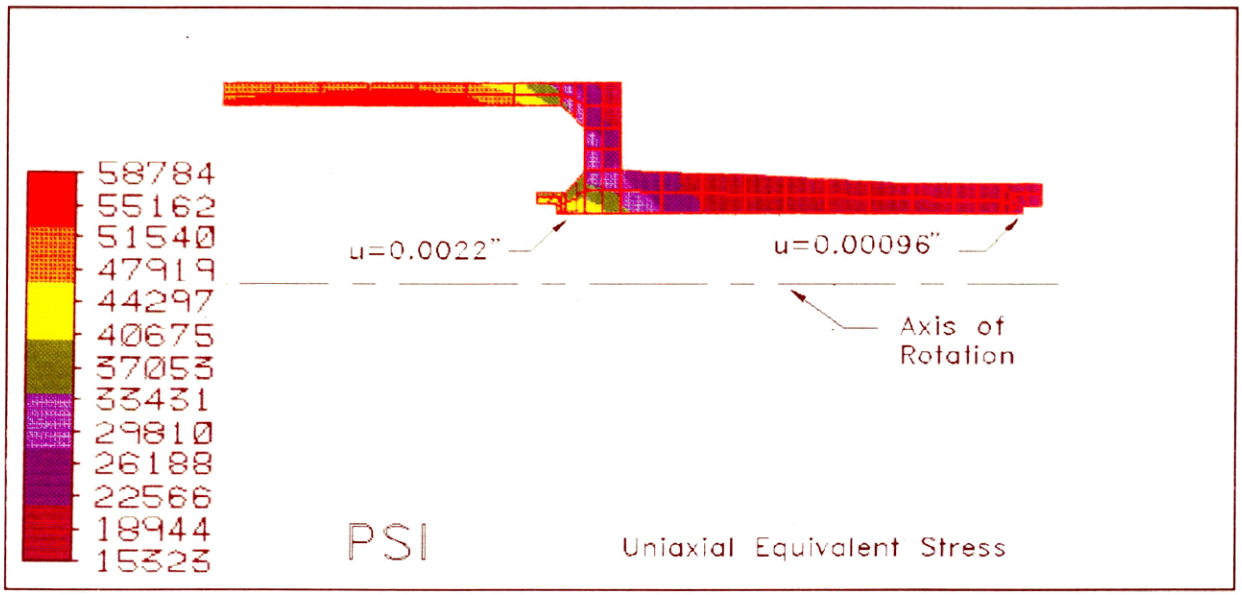

Figure 5.6: FEA of Axisymmetric Rotor With No Magnets, Rotating at 30,000 RPM

Since this difference (0.0001 in.) is smaller than the required machining tolerance of the part, it was determined that the analytical solution will provide adequate precision in computing the radial deformation at point "A", as a function of speed. It is therefore unnecessary to perform multiple FEA iterations at various speeds to determine the radial clearance at point "A", as a function of speed.

Since it has been shown that the radial deformation at

point "A" can be modelled using the analytical solutions, it is obvious that this method will also be valid at point "B". In fact, using the dimensions of the rotor at point "B" in Equation 2.1 yields 0.00098 in. radial deformation at 30,000 RPM. Comparing this value with the result found in Figure 5.6, it can be seen that the difference is 0.00002 in. (20 microns). Once again, the analytical solution can be used to determine the rotor radial deformation at point "B", as a function of speed.

Hooke's law states that the stress in a linear elastic, homogeneous material is proportional to strain. It can be seen that the uniaxial equivalent stress generated using Equations 2.2 and 2.3 closely duplicates the stress distribution in Figure 5.6. This is additional evidence that the radial growth analysis has been adequately accomplished. In essence, it has been numerically demonstrated that it is valid to use an analytical solution to model the deformation in this rotating body, as a function of speed.

5.3 Small Angle Approximation

A significant portion of the dynamic system calculations are based on the approximation that sine(θ) is equal to θ (measured in radians). Figure 5.7 displays the largest radial clearances that will exist between the bearing outer races and rotor inner surface. It is assumed that when contact occurs

between these components, additional angular deflection will be prevented. Based on these dimensions, the largest angle that will exist is 0.000661 radians. The sine of 0.000661 is 0.000661. There is no significant difference between these values, therefore the small angle approximation is valid in this analysis.

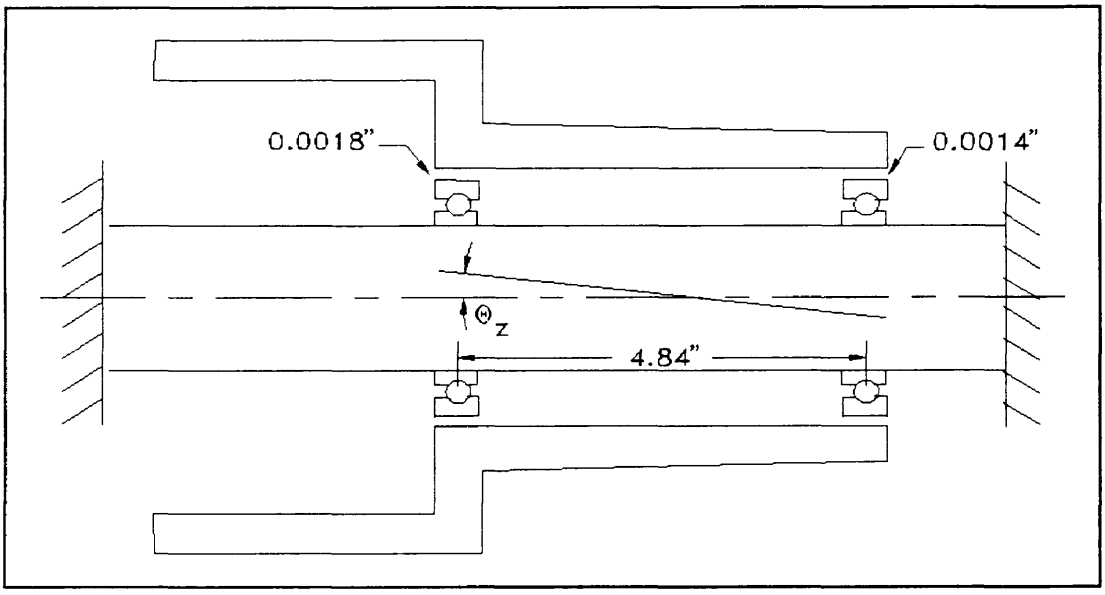

Figure 5.7: Maximum Rotor Angular Deflection

5.4 Natural Frequencies

In order to accurately model the total response of the rotor, it is necessary to apply the numerical and analytical techniques presented in Chapter Three. This also implies that it is necessary to determine that the rotor under analysis behaves as a rigid body with respect to bending (within the normal operating speed range). The rigid body characteristic,

as well as the natural frequencies (or critical speeds) which are due to rotor flexibility, can be determined using the numerical techniques developed by Kim (7). Using his computer program, which computes the critical speeds of flexible rotors, it has been determined that the first critical speed (or bending mode) of the first rotor is approximately 421,000 RPM. The first critical speed of the second rotor is 233,000 RPM. Since the normal operating range of the rotor is between 15,000 and 30,000 RPM, which is less than 13% of these critical speeds, the shaft is considered to be a rigid body (with respect to bending). It is predicted that these critical speeds will create increased mechanical noise levels caused by forcing functions operating near 7.02 KHz and 3.88 KHz respectively (if the forcing functions exist).

Using the analytical techniques described in Chapter Three, the system natural frequencies corresponding with translation and wobble can be determined. It will be seen that each system is affected differently by increasing angular velocity. This difference should be expected, and is due to the radically different dynamic properties of each system.

5.4.1 First Rotor

By referring back to Figure 5.1, it can be seen that the first rotor has no flywheel mounted on it. Because the magnification factor varies significantly in the neighborhood

of the natural frequency, it is often convenient to represent the location of natural frequencies using the plot of magnification factor. Figure 5.8 is a plot of the magnification factors associated with the natural frequencies of the first rotor, assuming no metal-to-metal contact occurs between the rotor and the bearing. It can be seen in Figure 5.8 that the first damped natural frequency, which is described as wobble, exists at 4633 RPM. The second damped natural frequency, which is described as translation, exists at 9882 RPM. These frequencies, as well as all of the remaining data, were produced with the Fortran computer program BIGPIC.FOR (which was developed by the author). The method of determining mode shape description will be presented later in this section.

The data generated in Figure 5.8 is based on a damping ratio of 0.02 (damping ratio of steel). It is interesting to observe the speed dependence of the natural frequencies in Figure 5.9. The value of the first natural frequency (wobble) is 4569 RPM when the rotor is at rest. It increases as a function of angular velocity squared. The frequency of the wobble mode is affected to some degree, by an increase in the angular velocity, but the effect is not dramatic. The second natural frequency (translation) is not significantly affected by an increase in angular velocity. Intuitively, both of these trends appear to be logical. The wobble mode should be affected (by increasing angular velocity) to a greater degree

than the translation mode. This is due to the gyroscopic stiffening effect. However, due to the relationship of the inertial terms associated with this rotor (I_x=0.163 and I_z=0.927 in-lb-sec^2), it is not expected that the gyroscopic stiffening term will affect either mode significantly. Therefore, the system dynamic characteristics should not be affected significantly by increasing angular velocity. The angular velocity increases faster than the natural frequency, so this speed dependence is not a significant problem or benefit for this system.

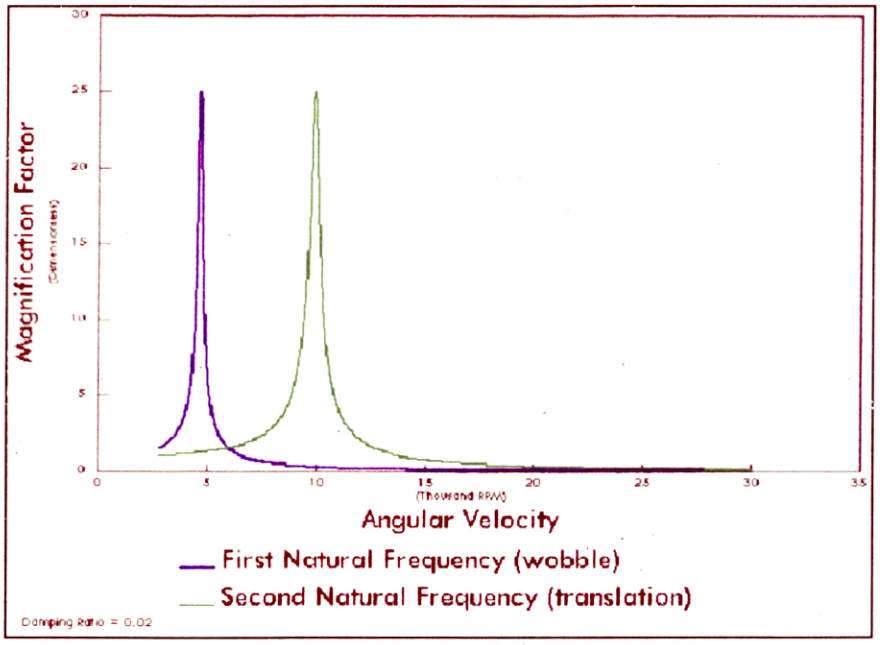

Figure 5.8: First Rotor Magnification Factors

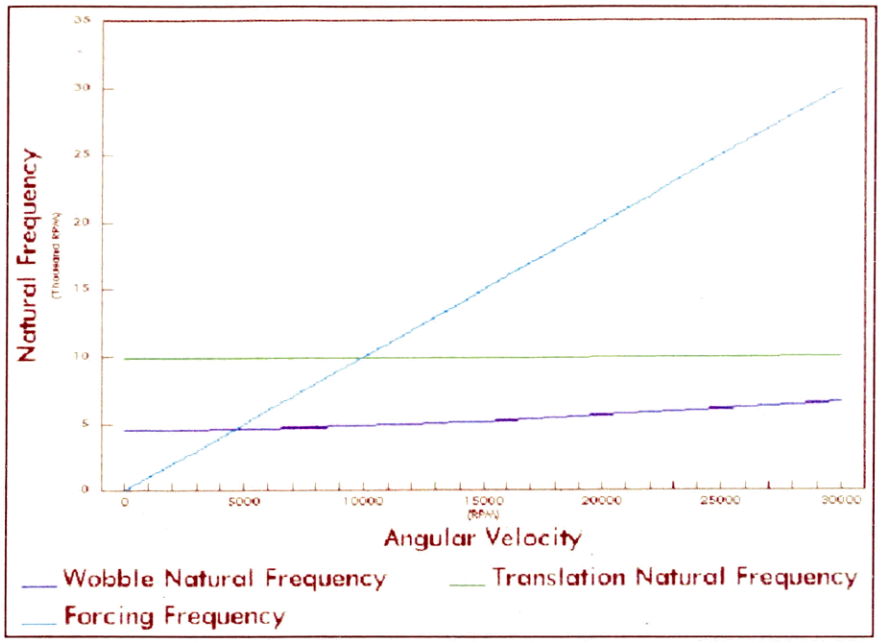

Figure 5.9: Speed Dependence of the First Rotor Natural Frequencies

According to these calculations, it is likely that the first natural frequency will be virtually invisible. In other words, the wobble natural frequency is not a critical speed for this system. There are three main reasons supporting this observation. First, the translation natural frequency is not numerically close to the wobble natural frequency. This will cause the magnification factor associated with the translation mode to be relatively small when the wobble mode is passed through. Second, it was assumed that there will be very little couple imbalance present in these rotors, which implies that there will be minimal wobble excitation. Finally, although this rotor does not benefit greatly from gyroscopic

stabilization, there is still some resistance to angular displacement of the principal centroidal axis. For these reasons, the forcing function that could excite the wobble mode will have minimal effect. If the wobble mode is observed at all, it will likely cause an increased mechanical noise level near 75 Hz (if a forcing phenomenon with that frequency is present).

The modal matrix, which contains the eigenvector coordinates that describe the first rotor mode shapes is:

$$[u] = \begin{bmatrix} y \\ \theta \end{bmatrix} = \begin{bmatrix} 1.0 & 1.0 \\ -0.569 & 0.081 \end{bmatrix}$$

Equation 5.1: Modal Matrix Describing the First Rotor

The first column represents the eigenvector coordinates associated with the first natural frequency (wobble). The second column represents the eigenvector coordinates associated with the second natural frequency (translation). The mode shape description is determined by comparing the second coordinates of these eigenvectors. Since the absolute value of the second coordinate of the first eigenvector is significantly greater than the second coordinate of the second eigenvector, it follows that the first eigenvector represents a significantly greater wobble tendency than the second.

5.4.2 Second Rotor

By referring back to Figure 5.2, it can be seen that the second rotor has a flywheel mounted on it (approximately centered between the bearings). In Figure 5.10 it can be seen that the first natural frequency of the second rotor exists at 5118 RPM. Its associated mode shape is described as translation. The second natural frequency, which is described as wobble, is never encountered in the operating range of this machine. This is because the gyroscopic stiffening effect causes the resistance to angular displacement of the rotor centroidal axis to increase with the square of angular velocity. As a result, the rotor becomes much more resistant

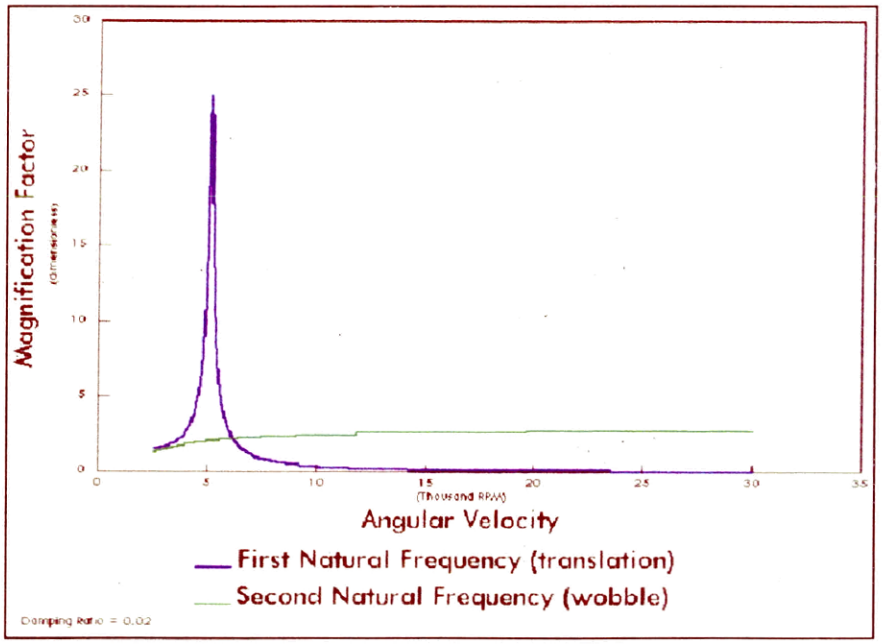

Figure 5.10: Second Rotor
Magnification Factors

to oscillation in the wobble mode and the associated natural frequency continues to increase. In fact, the natural frequency associated with the wobble mode of oscillation increases faster than the rotor angular velocity.

Inspection of Figure 5.11 reveals that the natural frequency associated with the wobble mode of oscillation, is 3139 RPM when the rotor is at rest. It increases in approximately a linear fashion throughout the operating speed range. The value of the natural frequency associated with the translation mode of oscillation, is 5176 RPM when the rotor is at rest. At approximately 3000 RPM, it decreases slightly to 5118 RPM, where it remains for the remainder of the operating speed range.

Once again, the natural frequency associated with translation remains relatively unaffected by an increase in angular velocity. However, the natural frequency associated with wobble increases significantly with increasing angular velocity. It will be seen that this phenomenon will have a profound effect on the dynamic response of this system.

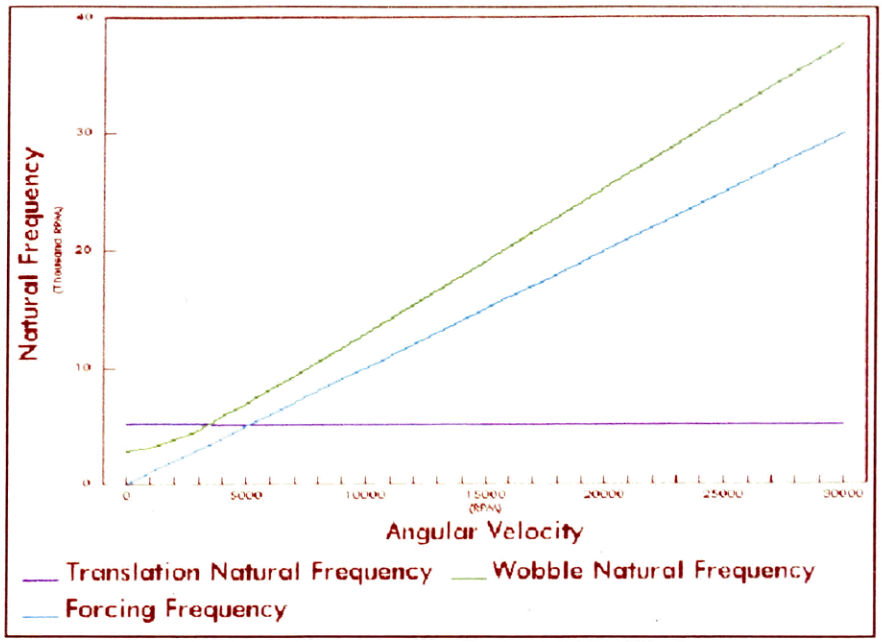

Figure 5.11: Speed Dependence of the Second Rotor Natural Frequencies

Because the second natural frequency is never encountered within the operating range of this system, the eigenvector describing that mode is never computed. It is known that the mode that is encountered is the translation mode, because the translation mode associated with this system is practically unaffected by the increased angular stiffness. Because the second eigenvector is not computed, the modal matrix is represented only by the eigenvector coordinates associated with the first natural frequency. Equation 5.2 is the modal matrix which describes the second rotor mode shapes.

$$[u] = \begin{bmatrix} 1.0 & -- \\ -0.024 & -- \end{bmatrix}$$

Equation 5.2: Modal Matrix Describing the Second Rotor

5.5 Dynamic System Factors

Because the natural frequencies of these two rotors are radically different, it follows that the effects which are computed using those properties will also be radically different. The magnification factor and phase angle associated with each natural frequency are the factors that physically represent the effects of each natural frequency.

The magnification factors and phase angles associated with the first rotor are presented in Figures 5.8 and 5.12. The shapes of the curves represented in these figures appear to be standard. Therefore it has been determined that the magnification factors and phase angles are being computed correctly, based on the correct computation of the natural frequencies.

The magnification factors associated with the second rotor are presented in Figure 5.10. The curve which describes the magnification factor associated with the translation mode appears to be standard. However, the curve which describes the magnification factor associated with the wobble mode flattens out at a value of 2.83 rather than peaking out, as is

observed of a conventional mode. Because the gyroscopic stiffening term causes the second natural frequency to remain above the rotor angular velocity, it is logical that the magnification factor associated with the second natural frequency would behave in this way also.

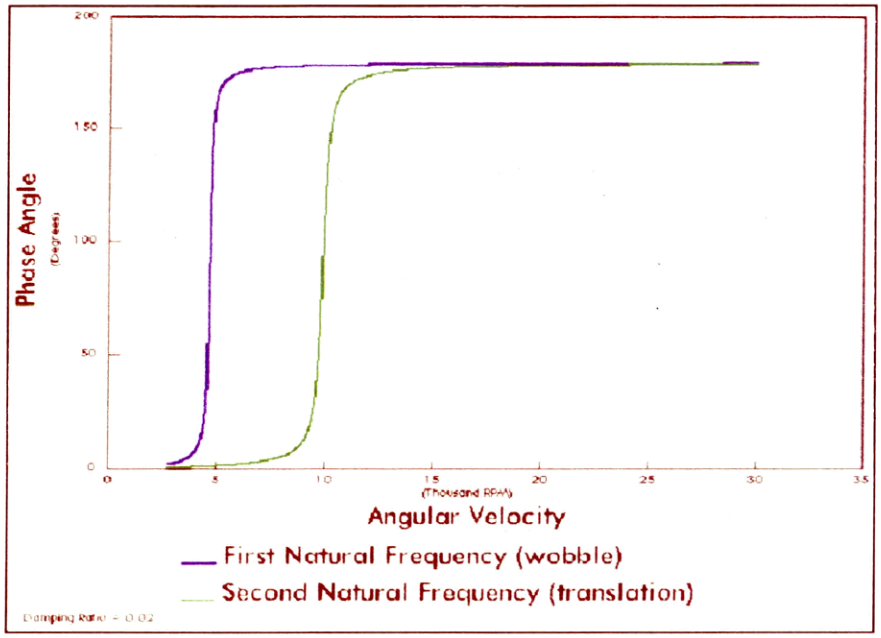

Figure 5.12: First Rotor
Phase Angles

The phase angles associated with the second rotor are presented in Figure 5.13. The curve which describes the phase angle associated with the translation mode appears to be standard. However, the curve which describes the phase angle associated with the wobble mode flattens out at five degrees. Once again, it is predicted that the gyroscopic stiffening

effect will have significant influence on the dynamic behavior of this system.

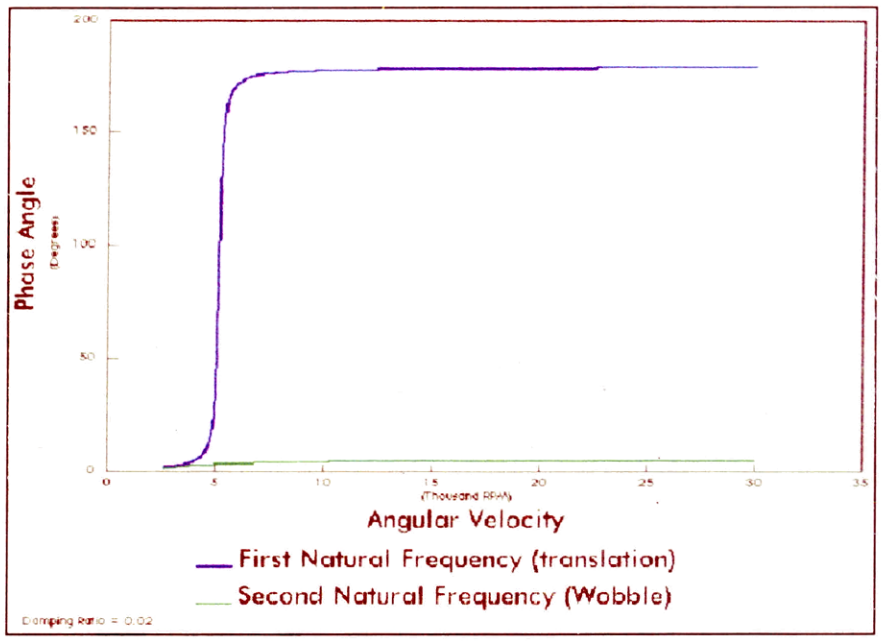

Figure 5.13: Second Rotor Phase Angles

5.6 Kinetic Effects

The effects which cause rotor support reaction forces are tightly inter-related. Rotor eccentricity, static dimensions and rotor dynamic properties will have strong influence on the operational characteristics of each system. Employing the techniques and boundary conditions presented in Chapters Two, Three and Four it is possible to quantify the rotor support reaction forces. Determination of these forces is essential to accurate prediction of the operational life or feasibility

of the machine.

5.6.1 First Rotor

Recall that the first rotor, which does not have a flywheel mounted on it, has approximately 0.0003 in. eccentricity, which is concentrated near the mass center (assumed to be a static imbalance). Figure 5.14 presents the steady-state rotor support reaction forces, as functions of rotor angular velocity. It can be seen that a peak centrifugal force exists at an angular velocity corresponding with the translational natural frequency. In a typical dynamic system,

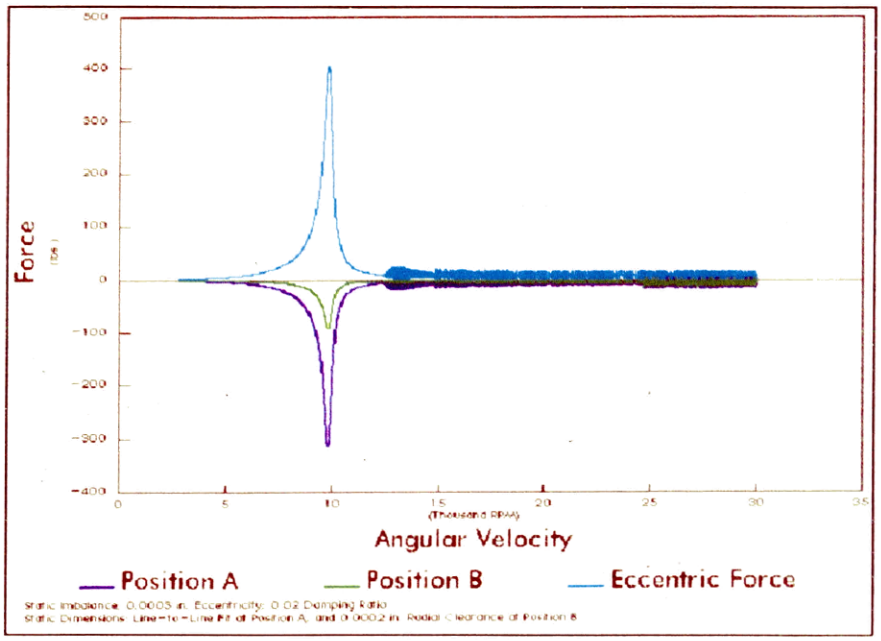

Figure 5.14: First Rotor
Reaction Forces

the centrifugal force would be nearly symmetric about the

natural frequency. This is because typically, the magnification factor is nearly symmetric about the natural frequency (see Figure 5.8). The peak in Figure 5.14 is not symmetric about the natural frequency. This is because the peak is a function of two effects. The magnification factor obviously has an effect on this system. Additionally, as the phase angle approaches 180 degrees, the rotor tends to rotate about its mass center. Since radial clearance exists between the bearing outer races and the rotor inner surface, the rotor is not fully constrained from this tendency of rotation about its mass center. Therefore, not only is the magnification factor decreasing, but the effective rotor eccentricity is also decreasing. Ehrich (11) has also predicted this non-symmetric centrifugal force profile in his studies of radial clearance within ball bearings.

The peak force of 400 lbs. is highly dependent on the system damping ratio. It is not clear at this time, what the damping ratio will be. It is conservative to use the damping ratio associated with steel, which is generally accepted as 0.02. However, this is really not an issue because damping only affects the rotor support reaction forces in the neighborhood of the natural frequency.

It must be understood that the peak bearing reaction forces displayed in Figure 5.14 are not valid. In fact, the forces will be significantly lower in the speed range between

5,000 and 10,000 RPM. This is because metal-to-metal contact will occur between the bearing outer races and rotor inner surface, during operation in this speed range. Calculations of bearing reaction force presented in Figure 5.14 incorporate the stiffness of the elastic interface between the bearing and rotor inner surface. Valid calculations would incorporate the stiffness of the bearing when metal-to-metal contact conditions exist. However, bearing reaction force calculations in the speed range between 12,000 RPM and 30,000 RPM are valid. This is because metal-to-metal contact between the bearings and rotor inner surface will not occur during operation in this speed range. Therefore, it is valid to use the stiffness of the elastic interface in natural frequency calculations, during operation in this speed range.

It is noteworthy that in all kinetic calculations, the sum of rotor support reaction forces is equal in magnitude and opposite in direction to the centrifugal force caused by rotor eccentricity. Considering Newton's laws of motion and the fact that these are steady-state conditions, these calculations would certainly be incorrect if this were not the case.

It can be seen in Figure 5.14 that the forces fluctuate slightly in the 12,000 to 30,000 RPM range. This is attributed to the marginal stability of the first rotor. Since the gyroscopic stiffening effect does not significantly constrain this rotor from wobbling, it will not exhibit the stability

associated with the classic gyroscope. Since a radial clearance exists between the bearing outer races and the rotor inner surface, the centrifugal force will fluctuate due to the change in the radial position of the rotor mass center. Stiffness of the device that connects the rotor inner surface to the bearing outer races will tend to prevent the rotor from rotating about its mass center. The radial displacement of the rotor mass center is limited by the radial clearance.

Referring to Figure 5.15, it can be seen that if excessive clearance exists as the translation natural frequency is passed through, it is possible that the rotor will not achieve the desired condition of rotation about its mass center. This is because if the rotor eccentricity is not greater than the radial clearance, then as the phase angle approaches 180 degrees, the centrifugal force will still be greater than the restoring force caused by operation in the super-critical speed range. The rotor will remain fully displaced until approximately 28,000 RPM. At this point, the gyroscopic effect will cause the rotor principal centroidal axis to be parallel with the axis of rotation. Coincidentally, it will also allow the restoring force of operation in the super-critical speed range to overcome the centrifugal force. As a result, the rotor will behave as desired from 28,000 RPM to 30,000 RPM. However, because the desired normal operating speed range is between 15,000 and 30,000 RPM, this is not an

acceptable operating range for this machine.

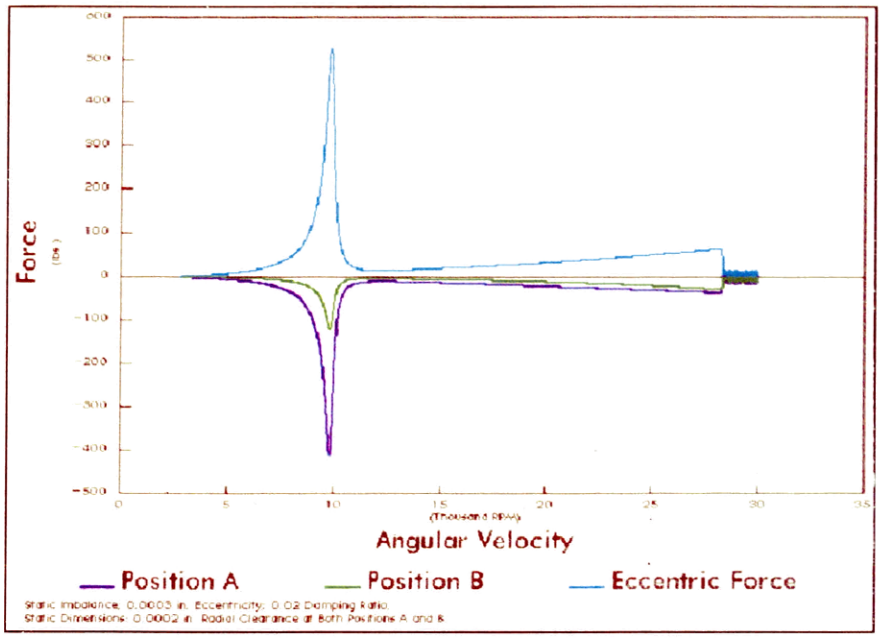

Figure 5.15: First Rotor Reaction Forces, If Excessive Static Radial Clearance Exists

5.6.2 Second Rotor

Recall that the second rotor has a flywheel mounted on it, and will experience a scheduled eccentricity that varies from 0.0003 in., to 0.001 in. at 30,000 RPM. It is also assumed that the imbalance will be located at the same axial position as the mass center (static imbalance). Figure 5.16 presents the steady-state rotor support reaction forces, as functions of rotor angular velocity. Once again, it can be seen that a peak centrifugal force exists at an angular velocity corresponding with the translation natural frequency.

The peak is symmetric about the natural frequency, as would be expected in a conventional dynamic system. The reason why this peak is symmetric while the peak associated with the first rotor is not, is that at 5,000 RPM there is virtually no radial clearance between the bearing outer race and the rotor inner surface. Therefore, the change in phase angle cannot cause the rotor to rotate about its mass center. The decrease in rotor support reaction force then, is only a function of the decreasing magnification factor.

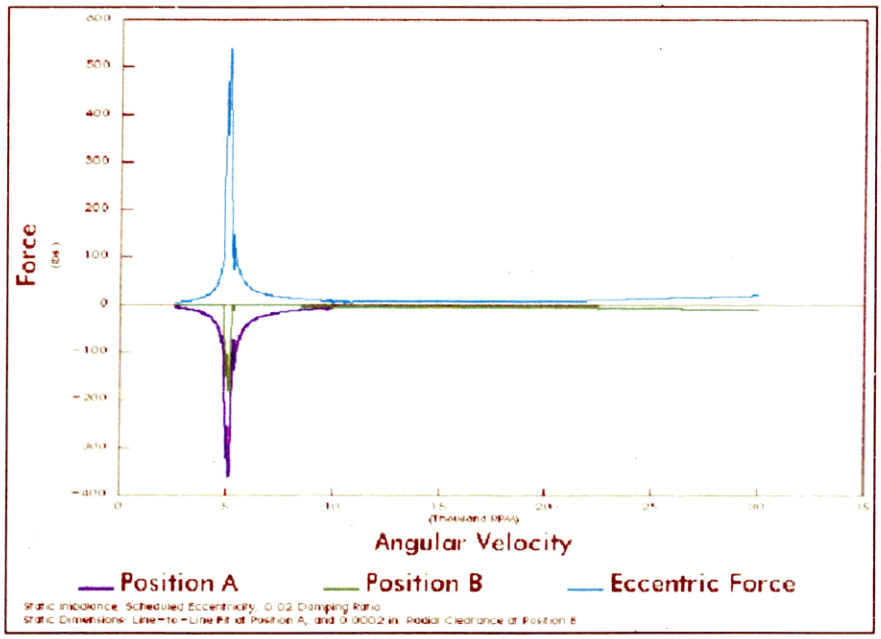

Figure 5.16: Second Rotor
Reaction Forces

Once again, it must be understood that the data generated between 0 and 12,000 RPM is invalid because of the metal-to-

metal contact conditions between the rotor inner surface and the bearing outer race (see Section 5.6.1). However, similar to the first rotor, the data generated between 12,000 and 30,000 RPM is valid because metal-to-metal contact conditions do not exist. It can be seen that above 20,000 RPM, the forces increase with an increase in angular velocity. This is because the rotor eccentricity is also growing, due to the non-uniform expansion characteristics of the flywheel (scheduled eccentricity). As a result, the stiffness of the device which connects the rotor inner surface to the bearing outer race causes the resistance to radial displacement to increase. The increase in forces will not have a negative impact on the operation of this machine.

By comparing Figures 5.14 and 5.16, it can be seen that this rotor will be much more stable than the first rotor. This is attributed to the gyroscopic stabilizing effect of the flywheel. Intuitively and analytically, this rotor will behave as a classic gyroscope. It will therefore possess the stable characteristics of the classic gyroscope.

5.7 Radial Clearance Including Kinetic Effects

Once the radial deformation and kinetic effects which describe this system have been computed, it is important to know how much clearance will exist between the bearing outer races and rotor inner surface. This is not only valuable as

a design tool, it is also useful in the validation of this analysis.

Before presenting the data, it is appropriate to define the terms "available clearance" and "floating clearance". Figure 5.17 is a graphic representation of these two terms. Available clearance is defined as the difference between the rotor inner radius (adjacent to the bearing) and the outer radius of the bearing outer race. This does not include eccentric forces transmitted through the bearing. Floating clearance is the distance between the bearing outer surface and the rotor inner surface, including eccentric forces that are transmitted through the bearing.

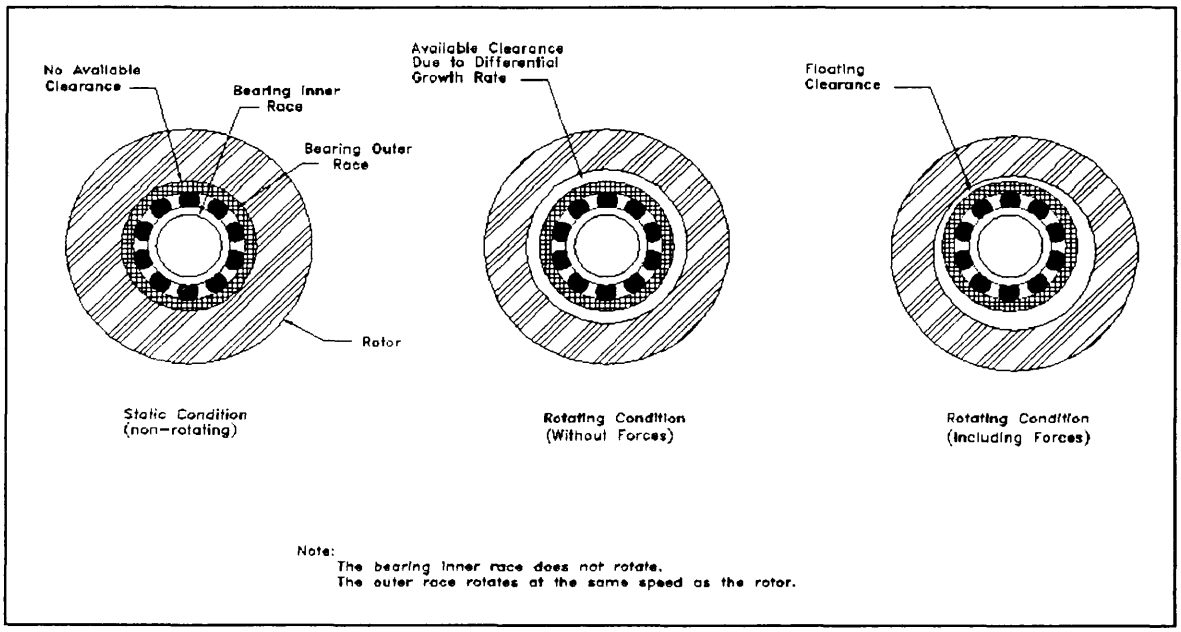

Figure 5.17: Available and Floating Clearance

Figures 5.18 through 5.21 characterize these radial clearances as discrete increments, resulting in a "stair-step" effect. Obviously, mechanical systems do not typically exhibit this sort of behavior. By inspecting the scaling of these graphs, it can be seen that each increment of radial clearance represents 0.0001 in. It is doubtful that calculating values in the fifth decimal place is valid, based on machining tolerance, etc. Therefore, the graphs have been left in their discrete forms.

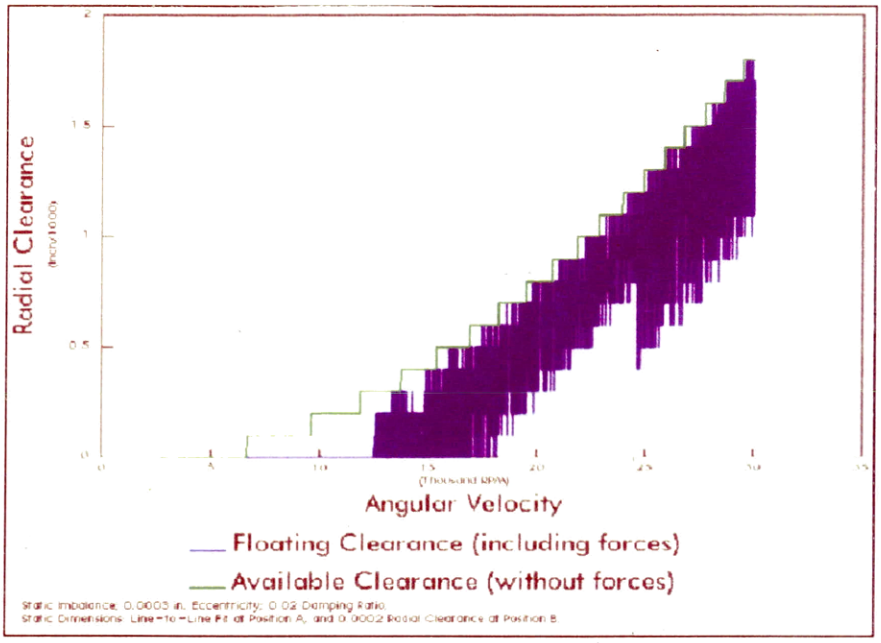

Figure 5.18: First Rotor Radial Clearance at Position A

Figures 5.18 and 5.19 present the available and floating clearances that will exist in the first rotor, as functions of angular velocity. It can be seen that the floating clearances

associated with the first rotor will be stochastic in nature. It may be more appropriate to describe the floating clearance as a range. Once again, this stochastic nature of the floating clearance is due to the limited gyroscopic stiffening, related to the first rotor.

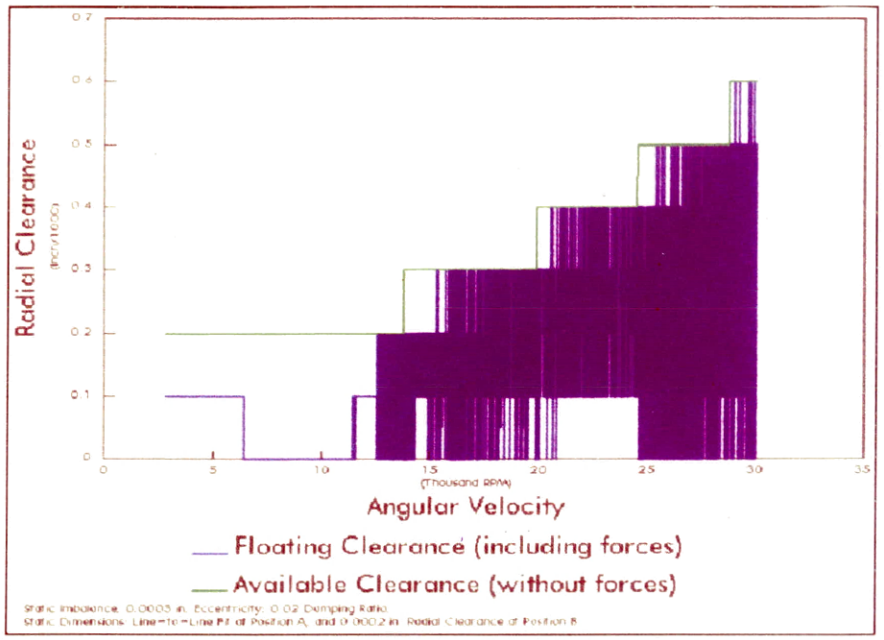

Figure 5.19: First Rotor Radial Clearance at Position B

Figures 5.20 and 5.21 present the available and floating clearances that will exist (at points "A" and "B") in the second rotor, as functions of angular velocity. It can be seen that the floating clearances associated with this rotor appear to be deterministic. It can be precisely predicted how much floating clearance exists as a function of angular velocity.

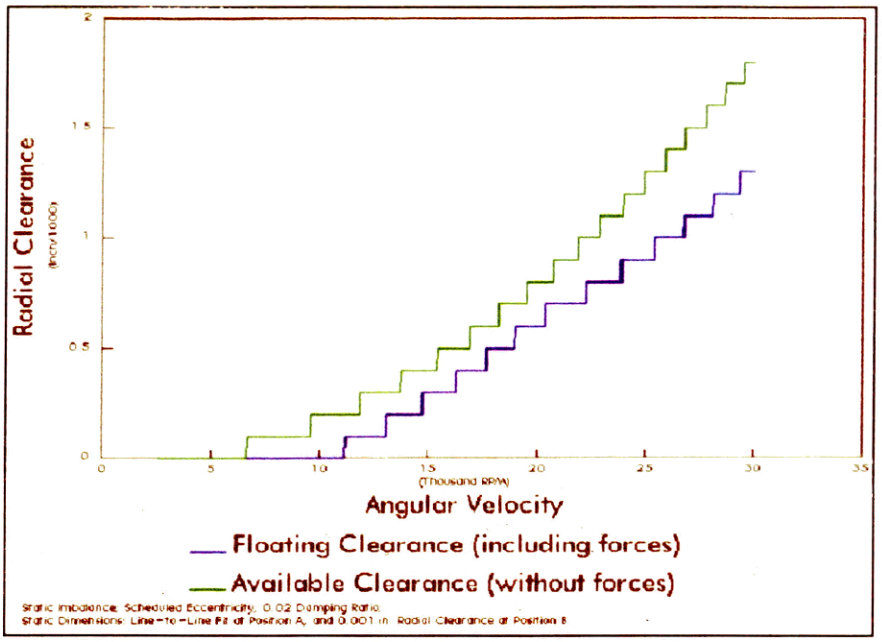

Figure 5.20: Second Rotor Radial Clearance at Position A

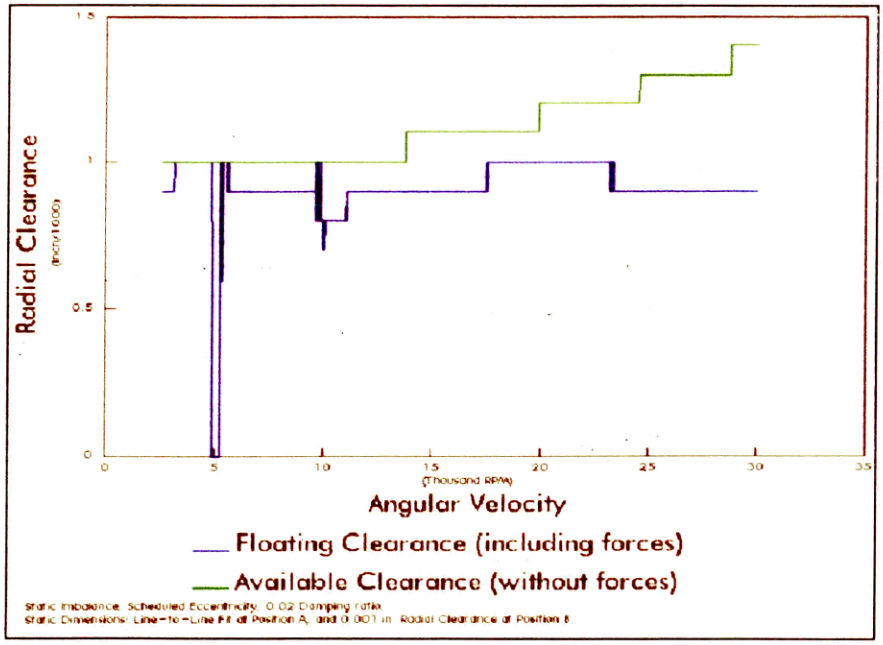

Figure 5.21: Second Rotor Radial Clearance at Position B

By comparing Figures 5.18 with 5.20, it can be seen that the available clearance at point "A" will be exactly the same in both rotors. The available clearance at point "B" has been increased because of the increased eccentricity in this rotor. The rotor will deform radially only 0.0004 in. at 30,000 RPM at point "B". However, the rotor eccentricity will be 0.001 in. at 30,000 RPM. It is therefore necessary to increase the inner diameter of the rotor at point "B", to allow the rotor freedom to rotate about its mass center. If the clearance were not increased at point "B" in the second rotor, metal-to-metal contact would occur within the operating range of the machine. This would decrease bearing life significantly.

In Figures 5.20 and 5.21, the floating clearance curve diverges from the available clearance curve at 20,000 RPM due to the increase in rotor eccentricity. This effect is was described in Sections 5.1 and 5.6.2.

It should be obvious that there can never be more floating clearance than available clearance. Similarly, there can never be negative available or floating clearance. Finally, floating clearance cannot be sustained until the available clearance is greater than the rotor eccentricity. All of these relationships are represented and satisfied in each of these figures.

It was mentioned several times in Chapters Four and Five that this analysis is no longer valid if the elastic interface

which is located between the rotor inner surface and bearing outer race becomes fully compressed, leaving no floating clearance. Figures 5.18 through 5.21 are useful for determining the validity of dynamic system calculations. In these figures, zero floating clearance indicates metal-to-metal contact between the bearings and the rotor inner surface.

Inspection of Figures 5.18 and 5.19 reveals that the first rotor, with its associated unbalance, may exhibit unpredictable behavior because contact between the bearing outer race and rotor will occur intermittently throughout the operating range. The nature of this behavior can be confirmed using the techniques of spectrum analysis and experimental modal analysis. Negative behavior will probably manifest itself as premature bearing failure or excessive mechanical noise. If the eccentricity is reduced, it is likely that the first rotor will behave more predictably.

Inspection of Figures 5.20 and 5.21 reveals that the second rotor will behave predictably throughout the system operational range. This statement is based on the fact that floating clearance will exist at both points ("A" and "B") throughout the operating range. Therefore, natural frequency calculations using the spring rate of the elastic interface are valid. It is possible to enhance this algorithm by incorporating natural frequency calculations which include

bearing stiffness (when appropriate). This improvement has been reserved for the future.

5.8 Remarks

The techniques developed in Chapters Two, Three and Four have been applied to the analysis of two radically different rotors. In fact, these techniques have been used as design tools to predict the feasibility and operational life of these proposed rotors. These rotors are currently being produced and will soon be tested. The results generated by this analysis will be confirmed experimentally.

Once again, numerical solutions have been employed to confirm the validity of development and application of analytical solutions, in order to describe the behavior of these systems. Several variations of the system dimensions and properties have been analytically tested. The results of those iterations have also been used to develop system sensitivity and tolerance for each variable. These tests are beyond the scope of this analysis, however it is noteworthy that the results were found to be in agreement with results presented in this document.

Chapter 6

CONCLUSIONS

6.1 Analytical Remarks

Generally speaking, the conventional analysis of high speed rotors often includes radial growth analysis, and possibly modal analysis. Complete and accurate rotor kinetic analysis is not as common. It appears as if the preceding analyses will provide the data essential to proper design and construction of a rotor having the given configuration (with the exception of thermal effects.)

Gyroscopic effects are often neglected in high speed rotor design. Depending on the rotor mass distribution and angular velocity, it may be valid to neglect these effects. However, it has been demonstrated that the resistance to angular displacement of the principal centroidal axis of a gyroscopic element can be adequately modelled as proportional to angular displacement, if the angle is small. Therefore, gyroscopic effects can significantly affect the dynamic response of compliantly mounted, rigid rotors.

In non-rotating 2 DOF systems, there exist two corresponding natural frequencies that remain relatively unaffected by operating conditions. However, since the gyroscopic element is modelled as a torsional spring (resisting angular displacement of the principal centroidal axis), and the

gyroscopic stiffening effect is proportional to angular velocity squared, the natural frequency corresponding with the wobble mode of oscillation can be significantly affected. The wobble natural frequency of the classic gyroscopic element will increase faster than the rotor angular velocity so that the system never passes through that natural frequency. Rotors which are described as long and slender do not benefit significantly from the gyroscopic stabilizing effect, and the wobble natural frequency remains fairly constant.

It has been demonstrated that if the wobble natural frequency is not numerically close to the translation natural frequency, the amplitude of the forcing function which excites the wobble mode will be small. Therefore, although the wobble natural frequency may be passed through, the mode will not be excited. In addition, even if the wobble mode is excited, the rotor dynamic response will not be detrimental to normal operations. This is because the wobble natural frequency has been designed to exist below the minimum normal operating speed of the machine.

Although the wobble mode in the two rotors presented does not appear to be critical in the rotor design, it is not valid to assume that the wobble mode will never be critical in rotor design. It is possible that the mass distribution and rotor support spring rates will cause the wobble natural frequency to be numerically close to, or even coincident with the

translation natural frequency. In that case the wobble mode could be critical to rotor design. In another case, if the wobble natural frequency is within the normal operating speed range of the machine, then excessive mechanical noise or vibration may be encountered. This could cause premature bearing failure.

It is a limitation of this algorithm, that the floating clearance must be greater than zero for the data to be valid. The existence of floating clearance at speeds less than the minimum operational speed is of little or no interest (because these conditions are not considered to be normal operational conditions). However, inclusion of bearing stiffness in natural frequency calculations (when no floating clearance exists) would expand the limits of valid calculations in this algorithm.

It is once again noteworthy that this analysis has not yet been experimentally proven. Numerical techniques were employed in the radial growth and modal analyses to demonstrate that the analytical solution techniques are valid. In addition, it does not appear as if any laws of mechanics have been violated or neglected. In the absence of experimental data, this is supporting evidence of the validity of those portions of this analysis. Confirmation of the proper analytical techniques will be attained during prototype testing.

6.2 Future Work

Analytical and numerical predictions have been made pertaining to the dynamic response of these two rotors. The prototypes will be fit with accelerometers, proximity sensors and thermocouples. The data obtained with this instrumentation will confirm radial growth, modal and kinetic characteristics of these systems.

Diametrically opposed positioning of the proximity sensors will confirm radial growth characteristics. Placement of accelerometers, immediately adjacent to the stationary bearing inner races will quantify the force transmitted from the unbalanced rotor to the stationary shaft. Comparison of the proximity sensor and accelerometer data will also provide information on the degree of decoupling supplied by the compliant bearing supports. Spectral analysis will be used to confirm the location of natural frequencies. Strategic positioning of thermocouples will provide data necessary to the development of rotor mechanical response to thermal effects.

After it is experimentally determined that the analytical techniques are correct, there are several additional features which could be added to this analysis. A dimension in time should be incorporated for two reasons. First, this would allow calculations of mechanical transient conditions. Rotor torque, and therefore angular acceleration could be added to

determine the total dynamic response due to both the steady-state and transient conditions. Second, after heat generation and dissipation data are collected, the dimension in time will also allow the calculation of steady-state and transient heat transfer conditions.

As it was stated in Chapters Four and Five, it is a limitation of this algorithm, that boundary conditions 1, 2, 7 and 8 (in Figures 4.5A and 4.5B) are incorrect. Once again, these boundary conditions are only applied if metal-to-metal contact between the bearings and rotor inner surface occurs. When this algorithm is enhanced, to include bearing stiffness (when appropriate), a more sophisticated method of computing gyroscopic effects which exist during these operating conditions must be developed.

It would be beneficial to re-construct the computer program (BIGPIC.FOR) in "C" programming language. Graphic representation of the desired rotor characteristics could then be developed. It would also allow for an active interface between the designer and the program. The designer could then alter the conditions seen on the display, to determine the stability margin of the rotor being analyzed.

REFERENCES CITED

1. Flannagan, R. C., M. Keating. Evaluation of A Flywheel Hybrid Electric Vehicle Drive. IECEC Meeting, August 1990, Reno, Nevada.

2. Eshelman, R. L. Flexible Rotor-Bearing System Dynamics. ASME Monogram, Volume 1 of 3. Library of Congress Index Number 72-92595, 1972.

3. Deutschman, Aaron D., W. J. Michels, C. E. Wilson. Machine Design- Theory and Practice. New York: Macmillan Publishing Co.,Inc., 1975.

4. Boresi, Arthur P., O. M. Sidebottom. Advanced Mechanics of Materials. Fourth Edition, New York: John Wiley & Sons, 1985.

5. Peery, David J., J. J. Azar. Aircraft Structures. Second Edition, New York: McGraw-Hill Book Company, 1982.

6. James, M. L., G. M. Smith, J. C. Wolford, P. W. Whaley. Vibration of Mechanical and Structural Systems: With Microcomputer Applications. New York: Harper & Roe, Publishers, Inc., 1989.

7. Kim, P. Y., R. C. Flanagan, I. R. G. Lowe. 1989. A New Method For The Critical Speed Calculation of Rotor-Bearing Systems-Part 1: Theory. In Rotating Machinery Dynamics, ed. T.S. Sankar, V. Kamala, P. Kim, and D.K. Rao, 71-76. American Society of Mechanical Engineers.

8. Flanagan, R. C., M. P. Marchand. Balancing and Dynamic Behavior of High Speed, Overhung, Fibre Composite Rotors. Ninth Machinery Dynamics Seminar. September 1986, Montreal, Quebec.

9. Eshbach, Ovid W. Handbook of Engineering Fundamentals. Third Edition, New York: John Wiley & Sons, Inc., 1975.

10. Greenhill, G. Gyroscopic Theory. New York: Chelsea Publishing Company, 1966.

11. Ehrich, F. F. Non-Linear Vibration in High Speed Rotors-Some Case Histories in Computer-Aided Vibration Analysis. Ninth Machinery Dynamics Seminar. September 1986, Montreal, Quebec.